Analysis

Evolving resource potential of glacial lakes with ongoing deglaciation

Georg Veh [1] ✉**, Wolfgang Schwanghart**[1]**, Oliver Korup**[1,2] **& Jonathan L. Carrivick** [3]

Melting and retreating glaciers are generating meltwater and creating space for new glacial lakes in Earth's high mountains. These glacial lakes become increasingly important freshwater reservoirs, but their value for hydropower, drinking water supply, tourism and ecosystem services over decades depends on their storage capacity and sedimentation-dependent lifespan. Here we estimate the volumes and sediment storage capacities for ~71,000 glacial lakes globally as of 2020. Combined, these lakes impound a water volume of $2,048^{+218}_{-296}$ km³ (median and 68% highest density interval), representing a $+12.7^{+9.1}_{-13.2}$% change compared with 1990. Half of the 2020 glacial lake water volume is located within 63 km of a coastline and below 200 m above sea level, mostly in sparsely populated, high-latitude regions such as Greenland, Arctic Canada, Patagonia and Alaska, where use of, and demand for, freshwater remains limited. The smallest lakes (<0.1 km²; ~80% of all) could lose 10% of their storage capacity within a century owing to sedimentation, while the 40 largest lakes, holding half of the global glacial lake volume, could endure for tens of thousands of years. These differing lifespans put pressure on a sustainable use of meltwater impounded within lakes, particularly in High Mountain Asia, where small glacial lakes could help serve the basic needs of millions of people, while unstable dams might rapidly remove some of this capacity. Overall, we offer regional and local baseline data of lake longevity to constrain a window of opportunity, in which growing demands for water security must be balanced with hazard mitigation and protection of rapidly evolving high-mountain ecosystems.

Ongoing global glacier mass loss is rapidly transforming high mountain landscapes[1]. Between 2000 and 2023, atmospheric warming caused glaciers to lose 6,542 ± 387 Gt (1 Gt = 10^{12} kg), forcing them to retreat to higher elevations at accelerated pace[2]. This trend is projected to continue throughout the twenty-first century and beyond, even if anthropogenic greenhouse emissions are halted[3]. By 2100, glaciers could lose another 26 ± 6% to 41 ± 11% of their mass as of 2015 (ref. 4). Thus, approximately 50,000 ± 10,000 km² of proglacial areas will emerge every decade on average in the twenty-first century, particularly in central Europe, Asia and the Andes, where only 5–20% of current glacial areas may remain[5].

Many expanding proglacial areas trap meltwater in the form of glacial lakes that can be dammed by abandoned moraines, outwash fans, glacier ice or bedrock riegels[6]. A recent global appraisal[7] mapped 71,508 glacier-fed lakes in 2020, covering 21,770 ± 544 km². Lake numbers and areas have increased globally by 54% and 11%, respectively, since 1990 (ref. 7). The timing and rate of glacial lake formation will determine how water quality (for example, temperature, salinity, turbidity or pollutants), aquatic habitats and biotic communities adjust both within lakes and in downstream rivers and coastal areas[6,8]. Meltwater from glacial lakes with permanent outlets is an essential water resource to millions of people in lower river reaches[9]. However,

[1]Institute of Environmental Science and Geography, University of Potsdam, Potsdam-Golm, Germany. [2]Institute of Geosciences, University of Potsdam, Potsdam-Golm, Germany. [3]School of Geography and water@leeds, University of Leeds, Leeds, UK. ✉e-mail: georg.veh@uni-potsdam.de
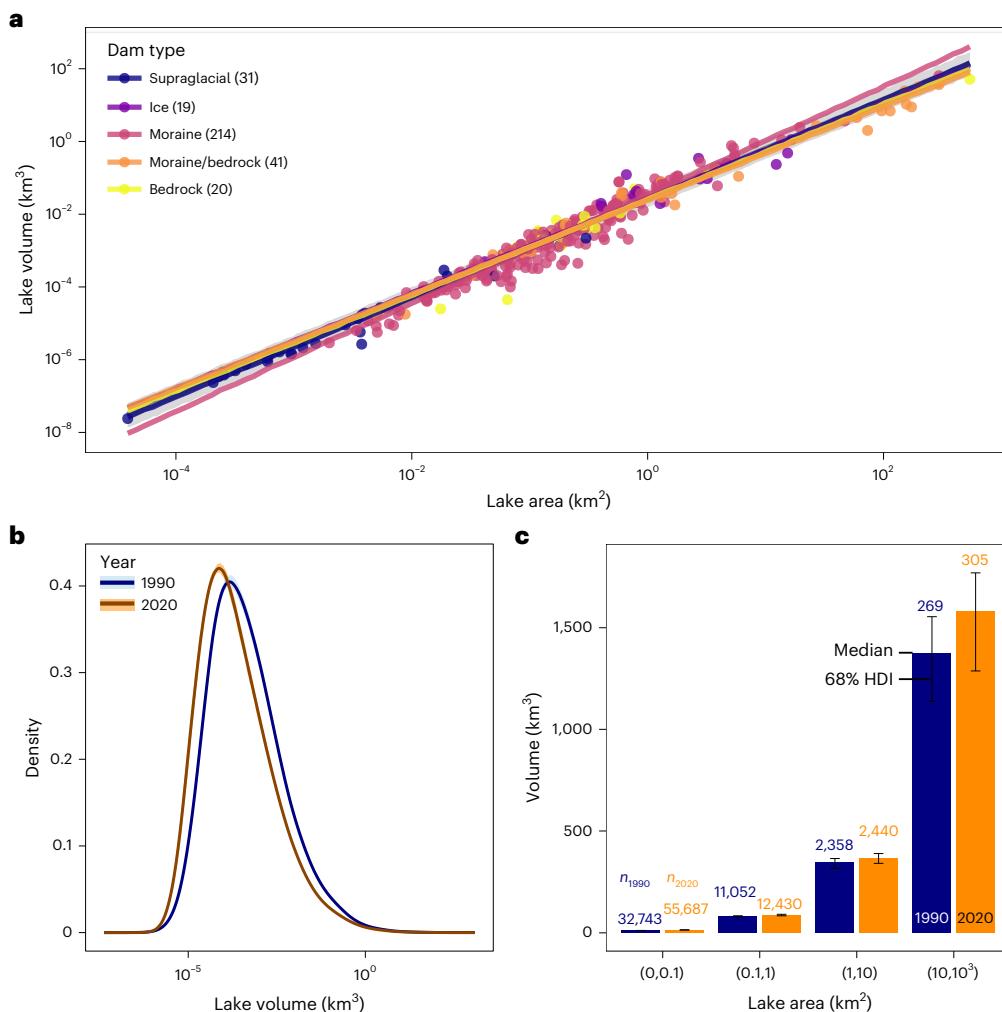
Fig. 1 | Empirical scaling method to estimate the global volumes of glacial lakes. a, Global compilation of 324 glacial lake areas and their bathymetrically derived volumes. Colours distinguish between five dam material types, with the sample size given in brackets. Lines show the posterior medians of the hierarchical regression of lake area versus volume; uncertainties are shown in Extended Data Fig. 1a. **b**, Median posterior probability density (thick lines) of individual lake volumes of all 46,422 lakes in 1990 (blue) and 70,862 lakes in 2020 (orange), including the 68% HDI (shade). **c**, Total lake volumes aggregated in four lake area classes. Bars show the median lake volumes per bin, and black lines indicate the 68% HDI for 1990 (blue) and 2020 (orange). Numbers above the bars represent sample sizes per bin.

some of these lakes have unstable dams, and their occasional failures have produced catastrophic glacial lake outburst floods (GLOFs)[10]. More than 1,700 GLOFs, primarily due to ice-dam failures, have been recorded worldwide between 1990 and 2023, resulting in hundreds of fatalities and substantial damage to hydropower facilities, infrastructure and farmland[11,12].

Hazards, risks and losses from GLOFs have motivated much of the previous research on glacial lakes[13–18]. However, glacial lakes also provide socioeconomic opportunities, including supplying drinking water, supporting industrial use or irrigation, and offering touristic services, such as producing artificial snow for skiing[19]. Lakes located within protected areas further offer tourism potential and alternative revenue sources for mountain communities[20,21]. In addition to their natural volume, lake levels can be raised by engineered dams to increase seasonal water storage, which can help mitigate water scarcity in drought-prone mountain regions such as High Mountain Asia[22] and the Andes[23]. Reinforcing lake outlets with pumps and turbines benefits the hydropower sector by offering flexible energy storage to help meet national targets in green energy production[24]. While the natural lake volume provides a first-order estimate of hydropower potential, its realization also depends on accessibility, including lake

elevation, climatic conditions and—especially in remote high-latitude regions—the distance from the coast to build new infrastructure for electrical grids.

Appraising glacial lakes as water resources requires an accurate quantification of glacial lake volumes. Yet, such volumes largely remain unknown; only a few hundred glacial lakes worldwide have been surveyed bathymetrically because of practical constraints and safety concerns. Hence, researchers have proposed various empirical lake volume–area (V–A) relationships[25–32] to estimate lake volumes. These models differ in their choice of model family, assumptions about lake geometry, and coefficient estimates, differences that partly reflect varying sample sizes (Methods). Most previous estimates based on V–A relationships have focused on predicting mean lake volumes, without explicitly accounting for the observed order-of-magnitude scatter in measured volumes in the prediction (Fig. 1a). Several factors contribute to this scatter: for instance, differing lake geometries reflect how glaciers with variable thicknesses and flow velocities have carved bedrock basins of diverse shapes and depths[33]. Dam characteristics such as height and material properties also control the maximum water storage capacity[25]. In addition, lake bathymetry evolves over time in response to lake age, changing distance from the parent glacier,

sediment accumulation, and the melting of dead ice within or beneath the lake bed[25,34–36].

Here, we propagate uncertainty in lake volume to refine estimates of regional freshwater potential, to assess changes in lake volumes related to glacier mass loss, and to project the lifetimes of glacial lakes. To this end, we compiled a catalogue of 324 glacial lake areas A and their bathymetrically determined volumes V (Supplementary Table 1) and fitted a hierarchical linear Bayesian V–A regression model that accounts for differences in dam types (Fig. 1a; Methods). We then predict the water volume (median and 68% highest density interval (HDI)), that is, the storage capacity beneath the lake surface, for all 70,862 and 46,422 glacier-fed lakes in 2020 and 1990 (ref. 7), respectively. These lakes were manually delineated by Zhang et al.[7] and classified as glacier-fed and dammed by moraines, bedrock, artificially reinforced dams or the glaciers themselves—either laterally or supraglacially—within a 10-km buffer around present-day glaciers from the Randolph Glacier Inventory (RGI, V7.0, circa 2000)[37] outside Antarctica. This buffer includes proglacial lakes both in contact with and detached from their parent glaciers, but excludes glacially formed lakes far from modern ice margins, such as the Great Lakes in North America. We then summed the posterior predictions of individual lake volumes to obtain the total and regional volume changes across the 18 glaciated regions in the RGI between 1990 and 2020.

Results

Global size distribution of glacial lake volumes

Based on the V–A model (Fig. 1a), we estimate that glacial lakes across our 18 study regions held a total of $2{,}048^{+218}_{-296}$ km³ (median and 68% HDI) of water in 2020 (Fig. 1b). For comparison, glaciers globally lost 273 ± 16 Gt yr⁻¹ between 2000 and 2023 (ref. 2), meaning that glacial lakes stored the equivalent of about 7.5 years of contemporary glacier mass loss. If all lakes were to drain into the world's oceans (area 3.625×10^8 km²), they would raise the global mean sea level by up to $5.65^{+0.6}_{-0.82}$ mm. However, 25% of all glacial lakes are located below 30 m above sea level (a.s.l.) with their beds partly below sea level[5], so the contribution to sea level rise is probably smaller. The distribution of all predicted glacial lake volumes is right skewed and peaks at 0.07 km³ (Fig. 1b). Overall, 80% of all glacial lakes cover areas <0.1 km², yet these small lakes collectively hold <1% of the total volume. A few large lakes dominate global meltwater storage: in 2020, just 305 glacial lakes >1 km² contained ~77% of the total volume, and the 40 largest lakes hold roughly half of the global glacial lake volume (Fig. 1c). For example, the largest lake in our sample, Lake Hazen on Ellesmere Island, Canada, accommodates a bathymetrically measured volume of ~51.4 km³ (from ref. 38; our estimate is 87^{+51}_{-63} km³) and, thus, 6.7% of the estimated global median glacial lake volume.

Disparate regional clusters of lake volumes

In 2020, more than two-thirds of the global median glacial lake volume were bound to only three high northern latitude regions, Greenland (616^{+74}_{-85} km³), Alaska (464^{+94}_{-88} km³) and Arctic Canada (312^{+62}_{-97} km³) (Fig. 2a). Smaller volumes are stored in the high southern latitudes, with Patagonia storing $12.4^{+2.0}_{-2.3}$% (245^{+41}_{-62} km³) of the global volume. Low-latitude regions, including the Northern Andes ($0.4^{+0.1}_{-0.1}$%; $8.5^{+1.6}_{-1.4}$ km³), the European Alps ($0.15^{+0.02}_{-0.02}$%; $3.0^{+0.4}_{-0.4}$ km³) and the three High Mountain Asia regions Asia Central, Southwest and Southeast ($1.1^{+0.1}_{-0.1}$%; 23^{+1}_{-2} km³), in combination account for only ~1.7% of the global glacial lake storage (Fig. 2a).

Present-day regional glacial lake volume scales with present-day total glacier volume (Extended Data Fig. 5a). Thus, regions that had and still have large volumes of ice such as the Greenland Periphery or Alaska[39] trap most of the glacial meltwater today. A notable exception is New Zealand, which has several large lakes in mountains with low glacier volume[39] (Extended Data Fig. 5a). This and other coastal mountain regions such as Greenland, Alaska, Patagonia and Northern Canada

accommodate the largest lakes in our sample, including Lake Hazen (Ellesmere Island, Canada), Tustumena Lake (Kenai Fjords, Alaska), Lago Greve (Patagonia, Chile), Lago el Toro (Patagonia, Argentina) and Lake Pūkaki (New Zealand). Most of these large water bodies are impounded by outwash plains and moraine ridges that predate the Little Ice Age, which was the most recent phase of glacier advance in the past millennium[40]. The overdeepenings that hold these lakes were probably carved multiple times during the Pleistocene, judging from dated lake sediments and moraines[41]. During the Last Glacial Maximum (LGM), 20–30 ka ago, glaciers extended beyond the mountains and onto forelands, reaching sea level or even out onto continental shelves[42]. Following the LGM, glaciers retreated during the Holocene, abandoning glacially scoured low-elevation basins and leaving space for some of the largest lakes in our sample.

Consequently, 50% of the glacial lake volume is below 200 m a.s.l. and <63 km from the ocean coast (Fig. 3). High-latitude coastal mountain ranges such as Svalbard and Jan Mayen, the Russian Arctic and Alaska have most of this volume close to sea level (Extended Data Fig. 6). Steps in this hypsometry of meltwater (Fig. 3, arrows) emphasize that few very large lakes retain much of the water volume near coasts. These lakes hold the largest potential as freshwater or hydropower reservoirs, but few are effectively used as such. One example is the hydropower dams of lakes Tekapo, Pūkaki and Ohau in South Island, New Zealand, that fulfil 25–40% of New Zealand's total electricity demand[43]. However, many other large lakes are located at very high latitudes with mean annual temperatures close to 0 °C and long seasonal lake ice cover. These harsh conditions will pose serious challenges to any economic use, in addition to suspended sediments in lakes that require filtering for hydropower or drinking water production[44]. Only 1.5% of the global glacier-lake volume lies above 3,000 m a.s.l., mainly in High Mountain Asia and low-latitude mountain ranges including the Andes (Extended Data Fig. 6). In those regions, the high potential energy of glacial lakes could complement river-damming for hydropower generation; however, hundreds of reported GLOFs raise concerns about the reliability and safety of harnessing this energy source[44,45].

Uncertainties in regional and local lake volume change

The largest lakes also contribute most to the uncertainty that remains in our global, regional and local estimates of lake volume change. While changes in lake areas can be determined with uncertainties of a few per cent[7], changes in volume need to account for the order-of-magnitude scatter in our empirical V–A regression model (Fig. 1a). Globally, the volume of glacial lakes has changed from $1{,}816^{+180}_{-272}$ km³ in 1990 to $2{,}048^{+218}_{-296}$ km³ in 2000 (Fig. 2b). However, uncertainty margins (here, the 68% HDI) for both years overlap and suggest no overall credible global change in lake volume ($+12.7^{+9.1}_{-13.2}$%), despite measurable increases in lake area ($+11$%)[7]. Only 7 out of 18 study regions (Alaska, Iceland, Svalbard, Caucasus and the three High Mountain Asia (HMA) regions) had a credible increase in their regional lake volume (Fig. 2b). The slightly negative volume change in northern Arctic Canada[7] is non-credible at the 68% HDI. Regional changes in lake volume correlate credibly with regional losses in glacier mass, that is, lake volumes have increased most where glaciers retreated the most (Extended Data Fig. 5b). Scandinavia and New Zealand had high increases in lake volumes even at moderate glacier mass losses as the storage capacity of glacial lakes was raised artificially following growing demands in hydropower energy[43,46].

Given the uncertainties in the hierarchical V–A model, only 1,625 (4%) out of 41,404 proglacial lakes (excluding supraglacial lakes) that existed in both 1990 and 2020 had a credible increase in volume by 2020. Collectively, these lakes grew by 618 km² in area (a third of the global growth in area) in this period, and relatively by 260^{+330}_{-100}% area per lake. The few credible gains in volume contrast with the widespread reported increases in lake area because substantial area change is required to yield a credible volume change given the large uncertainties
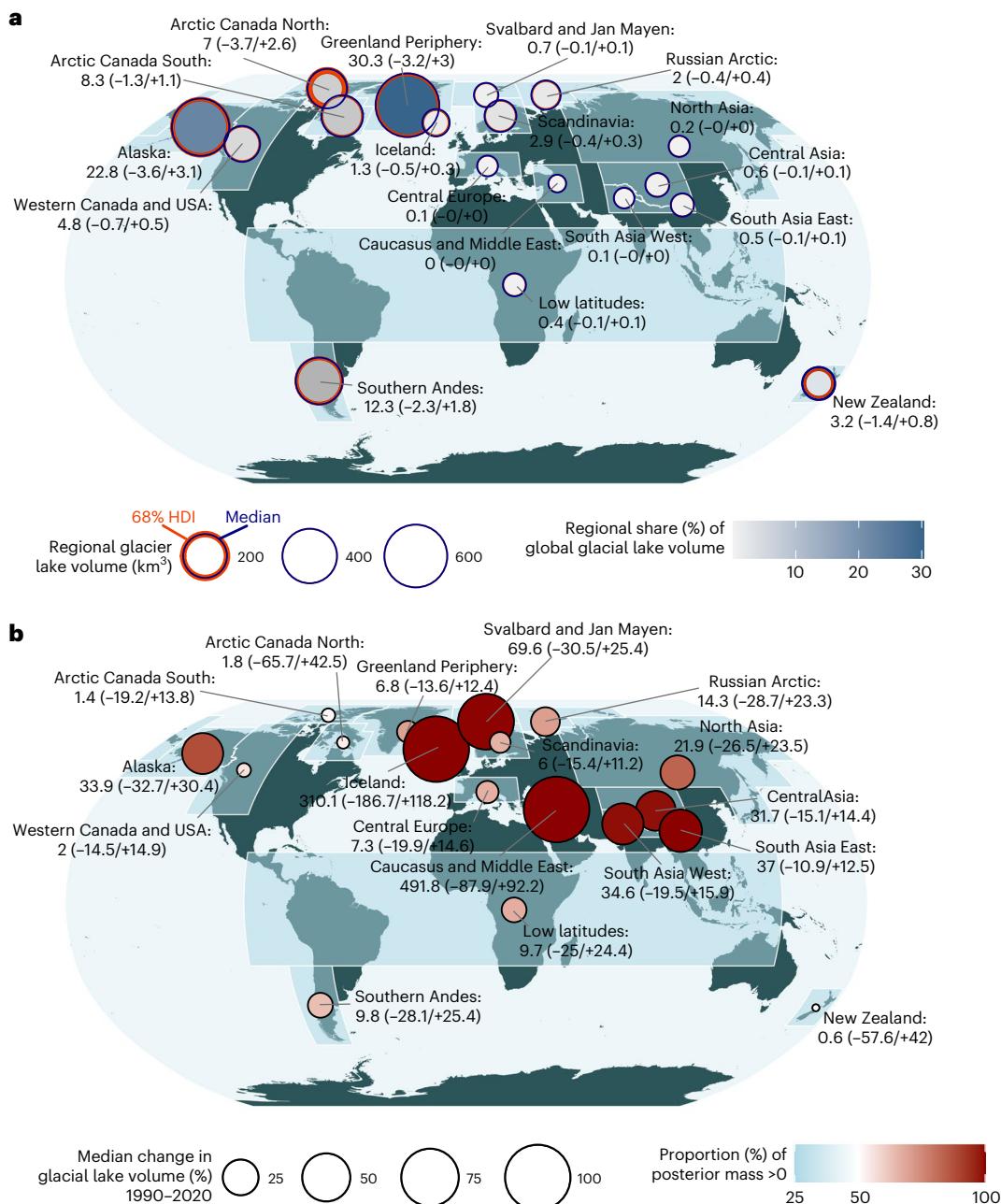
Fig. 2 | Regional lake volume (2020) and changes (1990–2020). a, Regional lake volumes and their global share in 2020. Bubble size (median in blue with an orange ring indicating the 68% HDI) is scaled to the regional lake volume for 18 RGI regions (semi-transparent polygons). Labels and bubble fill show the regional median share of the global volume along with the lower and upper margins of the 68% HDI. **b**, Percentage change in lake volume between 1990 and 2020. Bubble size is scaled to the median volume change, while bubble fill shows the proportion of positive posterior change. A posterior mass >50% (<50%) suggests higher credibility for an increase (decrease) in lake volume. Map created with QGIS with data from Esri, Global Mapping International, the US Central Intelligence Agency (The World Factbook) and Garmin International, Inc., provided by ArcGIS Data and Maps at the ArcGIS Hub (https://hub.arcgis.com/datasets/esri::world-continents/about).

in V−A scaling. Only 2 of the 40 largest lakes exceeded the 68% HDI threshold for volume change: one lake in Iceland, which was converted into a large hydropower reservoir during the study period, and one ice-dammed lake in Greenland, which has been continuously refilling after an outburst shortly before 1990. These cases represent some of the few physically plausible examples of volume growth for very large lakes that exceed model uncertainty. The growth of a few large lakes (>10 km²) clearly outpaces that of thousands of small lakes (<0.1 km²; Fig. 1c): overall, the 22,000 new small-sized proglacial lakes that formed between 1990 and 2020 contributed only ~2% (~45 km³) to the median global lake volume in 2020.

Limited lifetimes of small glacial lakes

High sedimentation rates in glacial lakes are part of the reason why the reported increase in lake surface area does not commensurately raise lake volume. Some of the highest sediment accumulation rates, spanning 10^1 to 10^3 cm yr^{-1}, have been observed at ice-contact lakes that receive debris from glaciers with high flow velocities and high subglacial erosion rates near the calving front[36,47,48]. Such lakes have probably become shallower during our study period despite their growth in surface area, whereas others might have grown in area, as the unchanged volume becomes gradually displaced upward. Contemporary sedimentation rates in proglacial lakes are poorly constrained
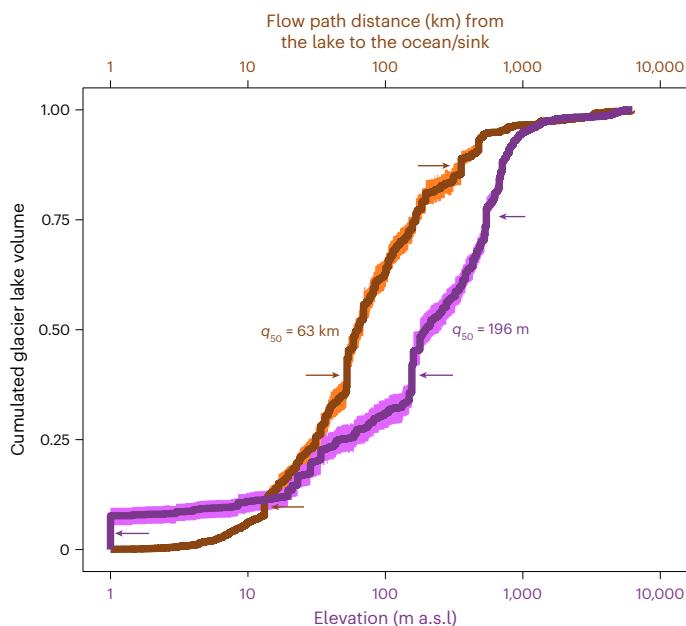
Fig. 3 | Global glacial lake volumes bound in low-elevation, coastal forelands. Cumulated glacial lake volumes ($n = 70,862$) are sorted by elevation (purple) and flow path distance (orange) to the ocean or sink, if lakes drain into endorheic basins ($n = 2,334$). Lines are the median cumulated volume, and shades are the 68% HDI. Colour-coded labels mark the elevation or downstream distance at which 50% (q_{50}) of the total volume is reached. Arrows indicate steps in the hypsometry.

because of difficult accessibility. The few available geomorphometric and sedimentary analyses suggest that even large lakes that formed after the LGM will eventually infill and be buried by extensive valley fills[49–51]. Hence, the lifespan of most small glacial lakes that form along with ongoing glacier retreat will probably be much shorter than the duration of the Holocene so far.

We model, to first order, the time until complete infill of all proglacial lakes as of 2020 (excluding temporary supraglacial lakes) by applying reported contemporary erosion rates[52] to their respective upstream catchments. We assume no intermediate sediment storage in floodplains, so annual catchment-wide erosion rates correspond to direct sediment yields into lakes. Our simulations account for uncertainties in lake volumes, sediment trapping efficiencies in lakes, rock and bulk sediment densities, and catchment-wide erosion rates (Methods). By weighting annual sediment production according to glacier cover, we acknowledge that ongoing deglaciation will drive a transition from predominantly glacial (higher) to fluvial (lower) erosion regimes[52] (Methods; Extended Data Fig. 7).

The simulated lifespans of individual glacial lakes cover nearly six orders of magnitude in years, with median values of ~200 years under glacial erosion rates and ~2,000 years under fluvial erosion rates (Fig. 4a). When weighted by glacier cover, the median lifetime is ~300 years, which is closer to the glacial scenario because 70% of the contributing catchments remain partly glacierized today (Fig. 4a and Extended Data Fig. 7c). Storage loss from sedimentation is primarily controlled by the initial lake volume, with small lakes projected to vanish much faster than large lakes. Accordingly, lakes <0.1 km² are projected to lose ~50% of their capacity by 2100 and may completely fill in during the twenty-second century, if they are fed exclusively by glacial erosion rates from their upstream catchments (Fig. 4b). By contrast, lakes >10 km² would lose only ~10% of their capacity during this millennium in this scenario.

Assuming much lower fluvial erosion rates[52] (Extended Data Fig. 7a), global lake storage loss is probably going to be delayed. Small lakes (<0.1 km²) may persist for >1,500 years until complete infill, while the

largest (>1 km²) could still retain ~75% of their volume until 16,000 AD—an interval comparable to the entire Holocene (Fig. 4c). These far-future projections exceed the intended design scope of our model, which assumes stationary erosion rates, no basin reorganization and no climate or glaciological feedbacks over centennial to millennial timescales; however, our simulations do emphasize the potential longevity of the largest glacial lakes in our sample. This idea is supported by seismic data from Alpine overdeepened basins, where >200-m-deep lakes often contain only 50–100 m of glaciolacustrine sediment deposited since the LGM[53]. Even under high local sedimentation rates (for example, >1 cm yr⁻¹; ref. 54), these large glacial lakes will be able to retain most of their capacity for tens of thousands of years, unless new glacial advances happen.

Lake longevity also varies by region owing to differences in the size distribution of glacial lakes. Regions with many small but few large lakes such as the Caucasus, European Alps, North Asia, South Asia West or Western Canada could lose half of their storage capacity during the twenty-second century under high glacial erosion rates, and ~10% even under fluvial erosion scenarios (Extended Data Fig. 8). Lakes with small storage capacities (<10⁴ m³) are projected to persist on average only for a few decades (Extended Data Fig. 10) or even shorter if filled by pulsed sediment inputs from expanding proglacial zones rich in unconsolidated debris[55–58]. Our projections support sedimentation scenarios for Swiss glacial lakes, which might lose 40% of their 2015 storage capacity by 2030 (ref. 59). Some 44–49% of Swiss lakes that might form due to glacier retreat during the twenty-first century are projected to be filled with sediments by 2100 (ref. 59). Episodic events such as GLOFs introduce further uncertainty to lake lifespans. Approximately 1% of all moraine-dammed lakes worldwide have (partly) drained during GLOFs in past decades[7]. The escaping flood waters can erode moraine dams, reducing their freeboard and leaving behind flattened basins. In the Cordillera Blanca (Peru), approximately 7% of all infilled lake basins that formed since the LGM probably drained catastrophically due to GLOFs[49]. Sediment accumulated over millennia in these drained lakes, greatly exceeding the volume of present-day lakes formed since the Little Ice Age[49]. Similarly, catastrophic mass movements such as rockfalls, avalanches, debris flows or landslides can rapidly fill lakes, particularly those situated near steep hillslopes, replacing millions of cubic metres of water with debris in a short time[60,61]. Ice-dammed lakes, by contrast, can fail repeatedly, and flood waters are able to evacuate substantial amounts of sediments from the lake floor. For example, repeated drainage of ice-dammed Lago Cachet 2 in Patagonia (Chile) during the early 2000s eroded ~25 × 10⁶ m³ from the lake bed, with local incision >40 m; today, the lake is gone as the ice dam has disintegrated[62].

An uncertain pathway of future lake development

The initial lake volume, the rate in upstream sediment supply, and abrupt drainage events contribute to the wide spectrum of individual lake lifespans, ranging from a few years to hundreds of thousands of years (Extended Data Fig. 10). While catastrophic outbursts curtail lake longevity, retreating glaciers expose new overdeepenings, often arranged in a cascade within a single valley system[59]. The most proximal overdeepened basins trap most incoming sediment[63], thereby extending the effective storage capacity and lifespan of downstream lakes. These downstream lakes may then largely depend on lateral sediment input from surrounding hillslopes, resembling the sediment-starved conditions observed in rivers downstream of hydropower reservoirs[64].

We estimate that, globally, 31% ($n = 21,911$) of all proglacial lakes are still coupled to their parent glaciers (Fig. 5). These lakes retain potential for further growth as their parent glaciers retreat through possibly even deeper subglacial troughs[33]. This growth potential varies by region: in continental regions such as High Mountain Asia and the Caucasus, 70–85% of all lakes have already detached from their glaciers, whereas more than half remain connected in Arctic Canada, Alaska and Iceland (Fig. 5). These figures suggest considerable scope for further lake expansion and sustained sediment trapping,
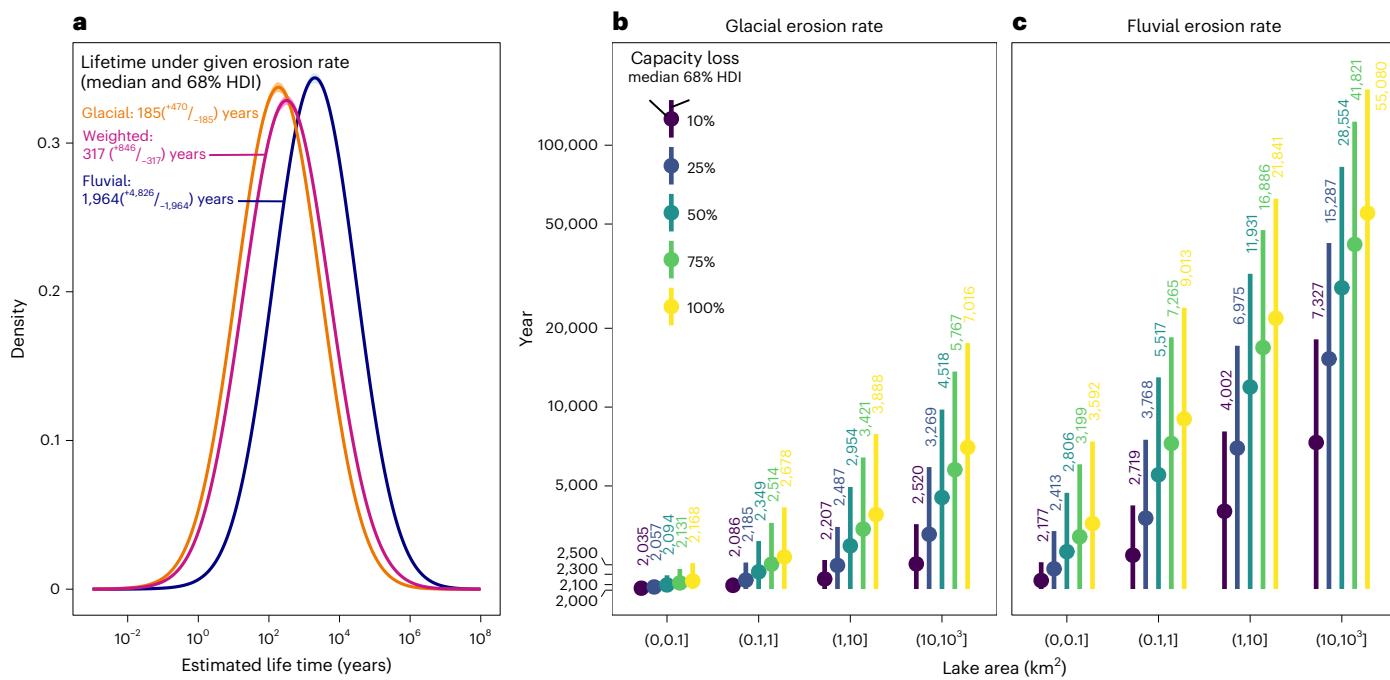
Fig. 4 | Lifetime and sedimentation-driven storage loss of glacial lakes.
a, Probability densities of estimated lifetimes for individual glacial lakes worldwide. We simulated the lifetime (period until complete infill) under three sediment supply scenarios: fully glacial, fully fluvial and an intermediate (Methods). Numbers show the median and 68% HDI of all simulated lake lifetimes. **b**,**c**, Projected year when lakes will have lost a given fraction of their initial storage capacity (as of 2020) due to sediment infill. Simulations assume sediment input from only glacial (**b**) or only fluvial (**c**) catchment-wide erosion rates, grouped by lake size intervals. Bubbles and numbers are the median year when 10%, 25%, 50%, 75% or 100% of lake volume will be lost; vertical lines show the 68% HDI.

particularly in highly glacierized high-latitude regions. However, detached lakes can also grow if they become clogged at their outlets or are recharged by groundwater, while others can desiccate in regions with high evaporation rates[65].

Anticipating the emergence, location and size of future lakes remains uncertain. In High Mountain Asia alone, some 13,000 additional lakes could emerge in an ice-free future, although estimates remain controversial due to assumptions in glacier thickness models and ice dynamics[13,66,67]. Judging from global land cover maps (Fig. 5; Methods), glacier cover upstream of existing proglacial lakes tends to increase with latitude, with the largest remaining ice masses concentrated in catchments at high latitudes (Arctic Canada, Alaska, Scandinavia and Patagonia). These regions also show some of the highest rates of glacier mass loss worldwide[68]. While glacier retreat exposes fresh debris sources that fuel high sediment fluxes, continued ice loss may eventually reduce sediment supply to downstream lakes in the future, especially if these retreating glaciers uncover more and more overdeepened sediment traps upstream. Meanwhile, some catchments in our sample are undergoing colonization by growing mosses, lichen, grassland or forests. For instance, ice-marginal areas in Greenland have doubled in vegetation cover since the 1980s, while bare bedrock surfaces have slightly decreased[69]. Yet, it remains unclear how such vegetation changes upstream will affect sediment input into lakes. In HMA, fluvial sediment yields from glacierized catchments both increased and decreased with expanding vegetation cover, while the role of growing lakes in this sediment cascade remained unassessed[70,71].

Contrasting human exposure to glacial lakes
Glacial lakes account for only ~1.1% of the global lake volume (181×10^3 km^3)[72]; however, they serve as important freshwater reservoirs in mountains where alternative water sources can be scarce and costly. Glacial lakes are embedded in remote, largely pristine and ecologically sensitive landscapes. Based on four global population datasets

(Methods), only an estimated 160,000–930,000 people live today in catchments upstream of glacial lakes (Fig. 6a). The low human presence upstream supports the generally high water quality of glacial lakes, especially where they lie in protected areas such as national parks or World Heritage sites[5]. HMA hosts most (30–68%) of the global population living upstream of glacial lakes, but has only ~1% of the global glacial lake volume, highlighting the region's disproportionately high pressure on limited lake resources (Fig. 6b). Here, water quality in glacial lakes is increasingly degraded by long-range atmospheric deposition, nearby settlements and tourism, resulting in elevated levels of microplastics, industrial chemicals and trace metals in lakes[73,74].

Despite generally low upstream population densities, runoff from glacial lakes attains growing importance downstream. Our analysis shows that the number of people living within 1-km wide and 50-km long buffers along rivers originating from glacial lakes is an order of magnitude higher (7.4–12.1 million) than for the catchment upstream (Fig. 6a). HMA also stands out with a high downstream population count (4.3–7.9 million people or 56–65% across all regions) that is in high demand of energy and freshwater (Fig. 6c). Hydropower potential from damming glacier-fed basins is highest in these regions globally[22], while increasing lake volumes and a long history of GLOF disasters have raised concerns about the sustainable use of, and safety for communities downstream of, these water resources. By contrast, Arctic regions such as Greenland, Iceland and much of the Canadian and Russian Arctic remain sparsely populated both upstream (0.03–0.4% of the global population upstream) and downstream (0.03–0.04%), suggesting minimal current anthropogenic influence or exploitation of glacial lakes (Fig. 6b,c).

Discussion
Common goods to protect or to use
Our study addresses a critical knowledge gap by estimating both the volume and sedimentation-based lifespan for tens of thousands of individual glacial lakes. We explicitly propagate the predictive uncertainty
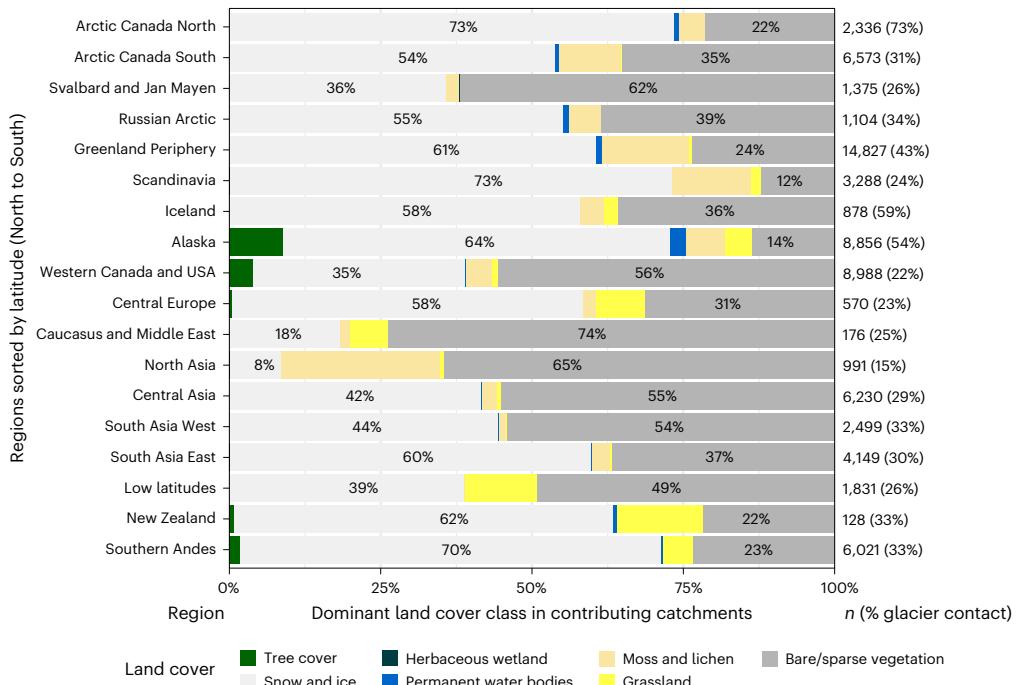
Fig. 5 | Dominant land cover in catchments feeding glacial lakes. We identified the most abundant ('dominant') land cover class in each catchment upstream of glacial lakes across 18 study regions using ESA WorldCover maps, version 2 (https://worldcover2021.esa.int/). Percentages are shown for the classes 'Snow and ice' and 'Bare/sparse vegetation' only. Numbers on the right indicate the sample size, along with the percentage of glacier-coupled lakes per region.

in lake storage potential using a Bayesian framework and offer a global appraisal of how long these lakes are likely to persist. Large residual scatter in the V–A relationship and reported erosion rates widen the prediction for individual lakes, underscoring the challenge of predicting the volume and lifetime from their surface extent alone. Yet, even under modest upstream erosion rates, most small lakes (<0.1 km²) are ephemeral and could lose ~10% of their storage capacity to sediment infill within the next century. By contrast, a small number of large, deep lakes may persist for millennia. These lakes hold a disproportionate share of the total volume and offer the greatest potential for long-term use in water supply, flood regulation, biodiversity conservation and recreation[75]. Large lakes also contribute most to the annual values from an ecosystem services perspective, which are estimated as US$33,447 ha^{-1} yr^{-1} (ref. 75). Taken at face value, glacial lakes may contribute services worth of US$72.8 billion yr^{-1} globally, although difficult access probably lowers their average asset. Nevertheless, their value is expected to increase in the future as lake number and area increase while water demand downstream rises[76].

As glaciers continue to melt and retreat, glacial lakes may take over their role as high-mountain 'water towers'[77]. In the Northern and Central Andes, Scandinavia and the European Alps, 23%, 37% and 97%, respectively, of all glacial lakes >1 km² have already been converted into hydropower reservoirs[11], and hundreds more hydropower schemes are planned or under construction close to lakes[44]. The Gornerli hydropower project in the Swiss Alps, for instance, plans to raise the water level of a small glacier-contact lake (currently <10⁵ m³) by an 85-m-high dam, creating a reservoir of approximately 150 × 10⁶ m³ at an estimated cost of approximately US$375 million. After its planned commissioning between 2030 and 2035, the project is expected to supply both hydropower (650 × 10⁶ kWh) and freshwater to around 140,000 households[78], one of the largest multipurpose water storage projects in glacier forelands worldwide. Using glacial lakes for hydropower production thus offers economic value, but only the largest lakes with low sediment input are likely to yield long-term stable returns. Most smaller lakes would require frequent and costly sediment maintenance work to remain functional[79]. In addition, reservoir purging may release previously

trapped pollutants such as mercury or black carbon into rivers, posing ecological and public health risks to downstream communities[80].

Any artificial damming, purging or water diversion must therefore be weighed carefully against potential ecological consequences. Emerging glacial lakes are rapidly colonized by microbial pioneers, algae, invertebrates and fish, initiating early stages of ecological succession in evolving habitats that may not have been ice-free for thousands of years[5]. Such young aquatic ecosystems are vulnerable to disruption from infrastructure that fragments water flow, sediment dynamics or nutrient supply. The potential economic benefits from glacial lakes must also be evaluated within legal frameworks, including property rights, water use laws, environmental regulation, landscape protection and hazard mitigation[65]. A prominent example is the 2003 conflict over Lake Shallap (Peru), where a multinational energy company began raising the water volume—previously lowered by the Peruvian government to reduce GLOF risk—by 2 million m³ to create a reservoir for hydropower[81]. Thousands of local residents protested the plan, citing safety concerns, ultimately forcing the company to abandon the project and lower the water level again without implementing a reservoir[81]. Policymakers and planners will thus need to navigate competing goals in the future: should growing lake volumes be harnessed for energy and water security, (partly) drained for GLOF mitigation or more strictly conserved as ecologically valuable systems? Seen as public goods, sustainable glacial lake management must balance multiple roles—from hydropower and tourism to ecosystem protection. Planning new infrastructure to facilitate access to or use of lakes should minimize disruption to habitat connectivity, species richness and food web structures, while compensating local communities for potential losses of ecosystem services[5,65].

Our estimates of glacial lake volumes and sedimentation-based lifespans provide a first-order decision-making framework to support regional assessments of freshwater provisioning and ecosystem services. In either case, the modelled distributions have wide tails, precisely where decisions become most consequential for practitioners. Acknowledging and reducing uncertainty in lake longevity is particularly relevant for lake management in arid high-mountain regions such
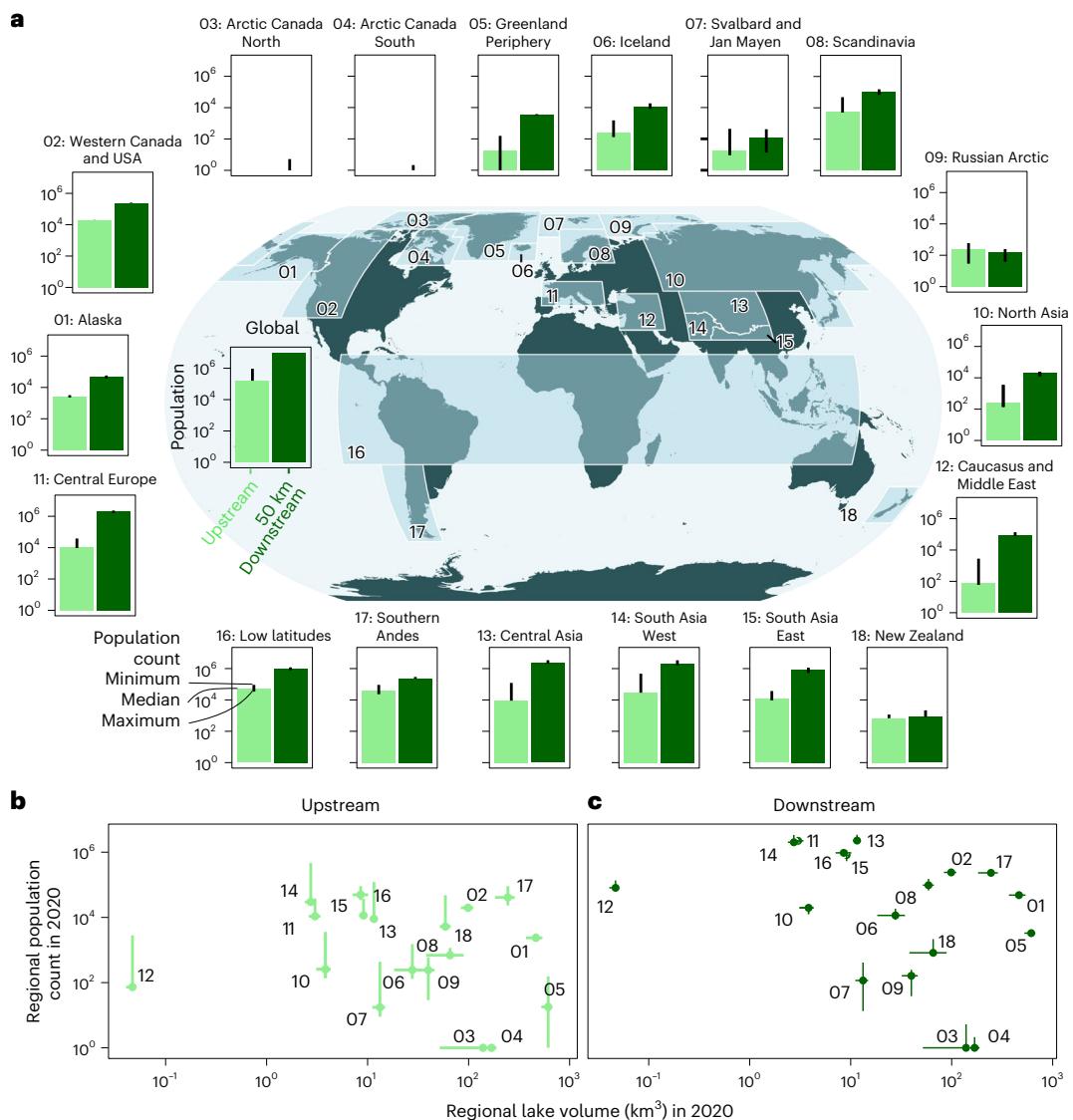
Fig. 6 | Population count upstream and downstream of glacial lakes.
a, Estimated number of people living in catchments upstream (light-green bars) and in a 1-km buffer in the first 50 km downstream (dark-green bars) of all 70,862 glacial lakes mapped in 2020 (ref. 7). Bar heights show the median regional population count; vertical lines span the minimum and maximum estimate from four gridded population datasets (Methods) in 18 RGI regions, shown by semi-transparent polygons and their regional codes in the central map. Polygons show the World Continents, a dataset compiled by Esri, Global Mapping International (GMI), US Central Intelligence Agency (The World Factbook) and Garmin, provided by ArcGIS Data and Maps at the ArcGIS Hub (https://hub.arcgis.com/datasets/esri::world-continents/about). **b,c**, Comparison between estimated regional lake volume and population count upstream (**b**) and downstream (**c**) of glacial lakes. Points show medians; vertical lines span the minimum and maximum regional estimated population count, and horizontal lines span the 68% HDI of regional lake volumes. Numbers refer to the regional RGI codes in **a**. Regional sample sizes and volumes are shown in Extended Data Fig. 9. Map in **a** created with QGIS with data from Esri, Global Mapping International, the US Central Intelligence Agency (The World Factbook) and Garmin International, Inc., provided by ArcGIS Data and Maps at the ArcGIS Hub (https://hub.arcgis.com/datasets/esri::world-continents/about).

as Central Asia and the Andes, where glacial lakes can play a key role in reconciling future conflicts over seasonal water shortages[9]. While future work may refine our estimated glacial lake volumes and lifetimes through improved models estimating lake bathymetry, subglacial topography and proglacial sediment connectivity, our global framework offers critical guidance for long-term water security, hazard assessment and ecological stewardship in deglaciating mountain regions.

Methods

Compiling empirical data on lake areas and volumes

We compiled an initial sample of 403 paired values of glacial lake area (*A*) and volume (*V*) from 92 literature sources (Supplementary Table 1). Lake volumes correspond to the documented survey year and were in most cases determined bathymetrically, either from single-depth

measurements or multibeam echo soundings. For 14 lakes, digital elevation models (DEMs) captured the lake fully drained following an outburst and volumes were derived from digitally refilling these lakes to the prefailure level. We classify the lakes into five dam-material categories: ice-dammed, supraglacial, moraine, bedrock and moraine/bedrock. The latter dam type refers to lakes occupying bedrock overdeepenings with associated moraine or outwash fans. We extracted the reported barrier type from the original reference and further interpreted it using high-resolution Google Earth imagery of the outlet structures. Our sample is restricted to lakes located within a 10-km buffer of the glaciers in the RGI[37], in accordance with the global glacial lake inventory used to estimate volumes for unsurveyed lakes[7]. In total, we compiled data for 324 lakes, 38 of which were repeatedly measured, and report the centroid coordinates and country for each case. From

our initial collection, we removed duplicate surveys—always selecting the largest reported area—to avoid autocorrelation and reduced variance in our catalogue[25]. Our sample size thus consists of 324 unique lake surveys, which more than doubles the amount of data that entered previous V–A models[82]. Uncertainties in reported A and V are rarely provided; when available, the underlying methods to derive them differ or remain unknown. To this end, we consistently use the mean reported A and V and assume negligible errors for both quantities. Accordingly, compiled lakes areas span seven orders of magnitude (3.9×10^{-5} to 5.4×10^2 km^2) and lake volumes nine orders of magnitude (2.4×10^1 to 6.4×10^{10} m^3) (Extended Data Fig. 1a).

Fitting a hierarchical lake area–volume regression model

We build on numerous previous studies showing that lake volume (V) can be approximated from lake area (A) using volume–area (V–A) scaling relationships (for a compilation, see supplementary information in ref. [82]). These empirical models rely on either exponential fits to raw data or linear fits to log-transformed data. Shugar et al.[26] and Zhang et al.[7] argued that applying a single model across the entire range of observed lake areas worldwide may overestimate the volumes of very large lakes. They proposed a piecewise approach: a linear model on log$_{10}$-transformed A and V for lakes smaller than 0.5 km^2 or 5 km^2, respectively, and an exponential or linear model on untransformed data for larger lakes. Our two main concerns with this approach are that (1) the models and residual distributions rely on different assumptions (exponential, linear or log-linear) on either side of the change point that are difficult to reconcile, and (2) the step between the two model segments creates a physically implausible increase in predicted volumes at the model breakpoint. These issues probably arise because large lakes—being less abundant in the sample and possibly having different dam structures, ages and infill histories—receive less weight in a pooled model that averages over all collated data. For example, large lakes in bedrock overdeepenings, sitting behind wide moraines or outwash fans from the LGM, may be shallower per unit area than those dammed by recently abandoned moraines.

Bayesian hierarchical models offer a flexible approach for capturing variation in the V–A relationship of lakes as a function of dam material type. The group-level structure allows parameters to be estimated jointly, with groups (that is, dam material types) informing each other through shared hyperparameters. Partial pooling shrinks group-level parameters towards the population mean estimate, a trait that is advantageous when sample sizes and variances differ across dam material types.

We fitted a hierarchical Bayesian linear regression on log$_{10}$-transformed pairs of lake area (in km^2) and volume (in 10^6 m^3), including their dam types as grouping structure. This transformation is important as it reduces the high skewness in the data, while forcing predictions to remain positive after back-transformation to the original scale, a prerequisite for our data. We modelled the probability of observing log$_{10}(V)$ from log$_{10}(A)$ using a robust Student's t-likelihood function, characterized by a mean μ, a positive scale parameter γ and ν degrees of freedom. The conditional distribution of lake volume V given lake area A is defined as

$$V_{ji} \sim t(\mu_{ji}, \gamma, \nu), \text{ for } j = 1, \dots, J \text{ and } i = 1, \dots, n_j \quad (1)$$

$$\mu_{ji} = \beta_{0j} + \beta_{1j} A_{ji}, \text{ for } j = 1, \dots, J \text{ and } i = 1, \dots, n_j, \quad (2)$$

where V_{ji} are reported lake volumes referring to the ith lake that is dammed by material type j. The mean μ_{ji} in the likelihood function is a linear combination using group-specific intercepts β_{0j} and slopes β_{1j} per dam material type j.

Approximating the posterior distribution benefits from scaled input data. Thus, we transformed log$_{10}(V)$ and log$_{10}(A)$ to have zero mean and a standard deviation of 1 before they enter the model.

Bayesian inference demands prior distributions for each model parameter, which are multiplied with the likelihood to obtain the posterior distribution. With the data centred on zero, we specified a normal, weakly informed prior for the intercept β_0 that has a mean of zero and a standard deviation of 1.5. The prior for the slope β_1 is largely positive using a normal distribution with mean of 1 and a standard deviation of 1.5, given the widely reported positive relationship between lake area and volume[25]. We refrained from using more informative priors, for example by taking parameters from previous studies, as most of their underlying data are also part of our compilation. The group-level standard deviations $\sigma_{\beta_{0j}}$ and $\sigma_{\beta_{1j}}$ model the uncertainty of β_0 and β_1 between the different lake types. We chose narrow normal distributions (mean of zero and standard deviation of 0.25), as we expect only moderate variance in the intercepts and slopes between lake types. The correlation across the group-level parameters is modelled through the Lewandowski–Kurowicka–Joe Cholesky correlation matrix; we set a prior on the scale parameter $\eta = 1$, which makes all correlation matrices equally likely. Further distributional parameters in the t-distributed likelihood include the scale parameter γ, which represents the unexplained variation in the model. Our prior for the scale parameter is a half-normal distribution with mean of zero and a standard deviation of 0.25 for scaled input data. Finally, we choose a normal distribution with a mean of 2 and standard deviation of 5 for the degrees of freedom ν (truncated at $\nu > 0$) in the likelihood function. Few degrees of freedom make the t-distribution heavy-tailed, thus better accommodating outliers in the data, while an infinite value of ν leads to the normal distribution. We fitted the model in the R package brms[83], which calls the Bayesian inference software stan in the background[84]. The model runs in 4 parallel chains, each with 4,000 iterations and 1,000 warm-up runs without thinning, resulting in 12,000 post-warm-up draws.

Evaluating the performance of the V–A model

We found no divergences after the warm-up phase, suggesting that the chains have converged (Extended Data Fig. 2). This is supported by the Gelman–Rubin potential scale reduction factor $\hat{R} = 1.0$ for all model parameters. In summary, the model suggests a strong linear relationship between scaled and log$_{10}$-transformed input pairs lake area and volume. The posterior regression slope on population level is positive with $1.35^{+0.06}_{-0.06}$ (median and 68% posterior HDI) for log$_{10}$-transformed lake areas and volumes (Fig. 1a). We found only moderate variation in the parameters among dam types, given the small standard deviations of both the model intercepts (median $\sigma_{\beta_{0j}} = 0.04$) and slopes (median $\sigma_{\beta_{1j}} = 0.1$). Moraine dams impound, on average, larger water volumes than other dam types, as indicated by higher group-level intercepts and slopes (Extended Data Fig. 1). We infer that moraine dams often sit atop overdeepenings with steep sidewalls, making glacial lakes behind moraine ridges deeper per unit area than ice- or bedrock-dammed lakes. Likewise, the residual variation is low, meaning that the predictor (lake area) explains much of the variance in lake volume. The degrees of freedom parameter in the Student's t-distribution remained low (posterior median $\nu \approx 4.85$), indicating that the model retained heavy-tailed residuals. This structure supports robustness to extreme observations and reflects the considerable residual variability even after log-transformation. While the prior on ν already favoured low values, the posterior of ν suggests that the data provided support for maintaining a heavy-tailed likelihood to accommodate persistent outliers.

For each observation that entered our model, we sample 1,000 draws from the posterior predictive distribution and compute the median prediction error, that is, the difference between the median predicted and bathymetrically derived lake volume. To this end, we retransformed the scaled and log$_{10}$-transformed predictions back to the original scale (Extended Data Fig. 1). To evaluate the performance of our model in light of the two other global appraisals, we summarize the errors in the predictions on either side of the suggested breakpoints at $A = 0.5$ km^2 (ref. [26]) and $A = 5$ km^2 (ref. [7]). Using three different error

metrics, we find that absolute and relative errors in lake volumes—whether evaluated on the original or $\log_{10}$-transformed scale—show no systematic over- or underestimation on either side of the suggested breakpoint. While some of the largest moraine or moraine/bedrock-dammed lakes (>5 km²) show higher absolute errors (Extended Data Fig. 3b), their relative and $\log_{10}$-scale errors remain comparable to those for smaller lakes (Extended Data Fig. 3a,c). The low prediction errors for large lakes indicate that our hierarchical model effectively balances error across the full range of lake sizes. Because large lakes dominate the total glacial lake volume (Fig. 1c), our global estimate of the lake volume in 2020 ($2,048^{+218}_{-296}$ km³) is approximately 60% higher than the previous global estimate of $1,280 \pm 354$ km³, despite using the same lake area data[7].

Predicting glacial lake volumes globally

We use this hierarchical regression model to estimate lake volume from lake area using a global inventory of glacial lakes, manually mapped from Landsat images for 1990 and Sentinel-2 for 2020 by Zhang et al.[7]. Several quality control measures, including a small minimum mapping unit (0.002 km²) and a large 10-km buffer around glaciers in the RGI, enhance the location accuracy and coverage compared with other global assessments[26,85]. From this inventory, we select all glacier-fed and ice-dammed lakes, and refined the 'glacier-fed' category by classifying lakes entirely within RGI glaciers[37] as 'supraglacial'. All other lakes in this category were randomly assigned as 'moraine-', 'bedrock-' or 'moraine/bedrock-dammed', reflecting the roughly equal shares of these dam types in high-mountain regions[86–89].

We compute 1,000 posterior draws of lake volumes ($\log_{10}\text{-}\hat{V}_i$) from the posterior predictive distribution for each lake mapped in 1990 and 2020. These draws inherently have higher variance than predictions based solely on the expected value of the posterior distribution as they account for residual error. We then back-transformed $\hat{V}$ to the original scale ($10^{\hat{V}_i}$). For individual lakes, we summarize the posterior predictive distribution in lake volume using the median and the 68% HDI. This choice of the HDI width is inspired by the one standard-deviation (1σ) error in frequentist statistics but can be widened (for example, to 95% or 2σ) to reflect greater uncertainty. For each region, we obtain a $n \times m$ matrix, where n is the number of lakes and $m = 1,000$ denotes the posterior predictive draws.

In Fig. 1b, we visualize the uncertainty in the shape of the lake volume distribution across posterior draws. For each draw, we predict lake volumes and apply a kernel density estimation (with a fixed bandwidth of 0.125 on $\log_{10}$-transformed volumes) to approximate the continuous distribution, yielding 1,000 density estimates. We then summarize these by computing the pointwise median and 68% HDI across all density estimates. To estimate the regional lake volume, we first sum across m, and then compute the median and 68% HDI over n (Fig. 2a). For all draws in a given region, we also ranked the predicted lake volumes and computed empirical exceedance probabilities to quantify how rare or extreme a given lake volume is relative to others in the same region (Extended Data Fig. 9). We then determined the number and proportion of lakes with median volume <10^6 m³ and >10^9 m³ (Extended Data Fig. 9). Finally, we estimated the absolute and regional volume change by taking the difference between the marginal distributions computed for 1990 and 2020. Again, we report the median and the 68% HDI of the differences in the posterior distributions (Fig. 2b).

Linking lake volume (change) to glacier volume (change)

We hypothesize that (1) the regional glacier volume scales with glacial lake volume and (2) regional glacier volume losses correlate with increases in glacial lake volume. To test these hypotheses, we use regionally aggregated estimates of ice volumes from Millan et al.[39], derived from an ice-flow inversion model calibrated for the period 2017/2018. In addition, we obtained regional estimates of glacier volume losses from Hugonnet et al.[68], who interpolated time series of

ASTER DEMs to quantify glacier elevation changes between 2000 and 2020. Both datasets refer to the RGI regions used in our analysis. However, glacier volumes in ref. 39 were aggregated for Alaska and British Columbia (RGI regions 01 and 02) as well as for High Mountain Asia (RGI regions 13, 14 and 15).

We fitted two linear regression models: one predicting the estimated mean regional glacier volume from the regional median of posterior-predicted lake volumes, and another one predicting regional glacier mass loss from the regional median of lake volume change. In both cases, we $\log_{10}$-transformed the response variables (glacier volume (km³) in 2017/2018 and glacier mass loss (km³) in 2000–2020) and the predictors (glacial lake volume (km³) in 2020 and glacial lake volume change (km³) in 1990–2020) to account for scale differences and potential nonlinear relationships. As in the hierarchical model above, we modelled the probability of observing glacier volume (loss) from lake volume (gain) using a robust Student's t-likelihood function. The conditional distribution of glacier volume (loss) G given lake volume V is assumed as

$$G_i \sim t(\mu_i, \gamma, \nu), i = 1, \dots, n \tag{3}$$

$$\mu_i = \alpha_0 + \alpha_1 V_i, i = 1, \dots, n, \tag{4}$$

where G_i is the median glacier volume (or glacier volume loss) in RGI region $i = 1\dots n$. The mean μ_i in the t-distributed likelihood is a linear combination using intercept α_0 and slope α_1.

We use identical priors for both models. The intercept α_0 follows a normal distribution with a mean of 2 and a standard deviation of 2.5. This choice reflects previous analyses indicating that present-day global glacier volume[39,90] is approximately two orders of magnitude greater than global glacial lake volume[7,26]. This large difference probably arises because only a fraction of retreating glaciers create suitable accommodation space for lakes, while others expose unconfined slopes and valley floors that cannot retain standing water or are simultaneously filled with sediments. Similarly, global glacier volume losses between 2000 and 2020 (ref. 68) exceed glacial lake volume gains[7,26] by about two orders of magnitude. The prior for the slope α_1 is a normal distribution with mean of zero and 2.5 standard deviations, ensuring that the modelled relationship between G and V can be both positive and negative. We use a normal distribution using a mean of zero and a standard deviation of 2.5 for the residual standard deviation γ, and a normal distribution with a mean of 2 and standard deviation of 5 for the degrees of freedom ν (with the probability mass truncated at zero to remain positive) in the likelihood function. As in the V–A model above, we fitted the model in brms using 4 parallel chains, each with 4,000 iterations and 1,000 warm-up runs without thinning, resulting in 12,000 post-warm-up draws. In both models, we found that the Markov Monte Carlo chains had converged (Extended Data Fig. 4a,b). Both cases have credibly positive posterior regression slopes, in line with our hypothesis of a correlation between glacier volume (loss) and lake volume (gain) (Extended Data Fig. 5).

Cumulated lake volumes with elevation and flowpath distance

We downloaded all tiles of the Copernicus 30-m Global Digital Elevation Model (GLO-30 DEM) via Microsoft's Planetary Computer data catalogue[91], using the rstac package[92] in R. The GLO-30 DEM, derived from TanDEM-X radar data collected during our study period (2011–2015), offers some of the highest terrain accuracy among global DEMs. For each lake within our 18 RGI study regions, we extract the median elevation from all DEM pixels intersecting the lake footprint.

We use TopoToolbox[93] functions in MATLAB to extract downstream flow paths from all lakes to the oceans or endorheic basins based on void-filled and hydrologically conditioned HydroSHEDS DEM that has a resolution of 15″ (~500 m)[94]. The data include drainage direction maps based on a D8 algorithm that account for endorheic basins.

Lake outlets were defined by snapping each lake's central coordinate to the nearest DEM pixel centre. From each outlet, we trace the downstream flow path by following the steepest descent, recording the coordinates, elevation and cumulative distance for each vertex along the resulting flow path. Where flow paths cross or flow along glaciers, the pathways modelled from the DEM may differ from the actual en- or subglacial drainage network. However, we assume that the overall length of the downstream flow path is only minimally affected by this discrepancy.

In Fig. 3 and Extended Data Fig. 6, we sort glacial lakes by their flow path length to the ocean or terminal sink in ascending order. We predicted 1,000 volumes per lake to calculate the cumulated lake volume as a function of flow path length. Similarly, we sort the lakes by their median elevation to obtain the cumulated lake volume as a function of lake elevation. From these cumulated curves, we report the median and the 68% HDI per percentile.

Estimating sediment infill and lifetimes of glacial lakes

Our idealized model of lake sedimentation is based on two key variables: the annual sediment production in the contributing catchment and the annual sediment deposition within the lake (Extended Data Fig. 7). We assume that annual sediment production is a function of the catchment area, erosion rate and rock density. Accordingly, lakes fed by large, rapidly eroding catchments receive greater sediment input. We delineated contributing catchments using the Upslope Area tool in SAGA GIS (V9.6.1), applied to the upstream, sink-filled DEM tile(s) of each lake. Catchment areas are then multiplied by an estimate of their erosion rate.

As in situ measurements of erosion rates are unavailable for each catchment in our sample, we rely on a compilation[52] of reported erosion rates with measurement timescales <500 years (n = 2,963) to approximate contemporary sediment production. In 92% of all cases, these rates were inferred from volumetric estimates, including dated deposits or sediment yields in rivers, while the remainder is from surface or detrital cosmogenic radionuclide dating[52]. Mean erosion rates differ by roughly an order of magnitude between glacial and fluvial environments, with means of −0.09 (0.81 mm yr^{-1}) for $\log_{10}$-transformed glacial and −1.12 (0.076 mm yr^{-1}) for $\log_{10}$-transformed fluvial erosion rates. The corresponding standard deviations on the $\log_{10}$-scale are 0.91 and 0.88, respectively. We estimated sediment production for both end-member scenarios, either fully glaciated or fully ice-free contributing catchments. Finally, we converted sediment production (in mm yr^{-1}) to annual sediment yields (in t km^{-2} yr^{-1}) using the contributing catchment area of a given lake and an empirical rock density distribution for sedimentary, igneous and metamorphic rocks (mean density μ_r = 2.6 t m^{-3}; standard deviation σ_r = 0.2 t m^{-3})[95] (Extended Data Fig. 7a).

Sediment deposition in the lake must also account for trapping efficiency and the lower bulk density of deposited material (Extended Data Fig. 7b,c). Some material bypasses the lake outlet, while deposited sediment typically has reduced bulk density. Trapping efficiency depends on discharge, flow velocity, lake geometry and water residence time in the lake[96]. A fraction of fine sediment may remain in suspension, whereas coarse bedload is effectively trapped in glacial lakes. Proglacial lakes and alpine hydropower reservoirs have very high reported sediment trapping efficiencies (80–90%)[55,56,63,64,97], with trapping efficiencies <50% being rare[63]. To approximate this high trapping efficiency, we used a beta distribution, a two-parameter probability distribution defined on the unit interval. We choose the parameter α = 9 and β = 3, thus assuming a mode of 0.8 in the beta distribution (Extended Data Fig. 7c). We also accounted for substantially lower bulk density of deposited sediment (μ_d = 1.6 t m^{-3}, σ_d = 0.2 t m^{-3})[98] compared with the rock density (Extended Data Fig. 7b).

We estimate the time to complete infill of each lake as the ratio of the initially available lake volume to the product of annual sediment production, sediment trapping efficiency and bulk density of the deposited material (Extended Data Fig. 7c). We excluded 11,772 supraglacial lakes from our simulations, as they may be poorly connected to the sediment cascade. For the remaining 59,090 lakes, we estimated a distribution of 'theoretical lifetimes'—that is, all human and environmental controls held constant—by drawing 5,000 random samples from the probability distributions of erosion rates, rock densities, trapping efficiencies, bulk sediment densities and posterior lake volume estimates. As a compromise between the two end-member scenarios, we also weighted the membership to either fully glacial or fluvial dominated catchment based on the present-day glacier cover of each catchment[37] (Extended Data Fig. 7c,d). These simulations of expected lifetimes were cumulated at global (Fig. 4) and regional scales (Extended Data Fig. 8), from which we derived probability density and cumulative distribution functions. In either case, we report the median and the 68% HDI of simulated lake lifetimes.

Catchment-wide land cover analysis

We intersect each glacial lake polygon with the glacier outlines from the RGI V7.0 to determine whether lakes remain in contact with their parent glaciers. For Greenland, we also used the outlines of the ice sheet (available at ref. 99), which is not part of the RGI. The resulting regional share of glacier-contact lakes (Fig. 5) should be considered a maximum estimate, as glacier outlines in the RGI were mapped in 2000, while the glacial lake inventory is from 2020; thus, lakes could have decoupled from their retreating parent glacier in the meantime.

To obtain the land cover in our catchments, we downloaded all available tiles of the ESA WorldCover V2 land cover maps (https://worldcover2021.esa.int/) intersecting with our study regions. These maps distinguish ten land cover classes, which were predicted from 10-m Sentinel-1 and Sentinel-2 data obtained in 2021, thus closely aligning with the timestamp of our glacial lake dataset in 2020. The WorldCover V2 maps have an overall accuracy of 83.8%, the highest of all currently available global land cover products[100]. For each upstream catchment, we extracted all land cover classes, and report the dominant, that is, the most frequent, land cover class per catchment in Fig. 5.

Estimating population upstream and downstream of glacial lakes

We extracted estimated population counts from two spatial domains: (1) upstream catchments draining into glacial lakes, and (2) a 1-km-wide buffer along river channels hydrologically routed downstream 50 km from glacial lakes. The choice of this downstream flow path builds on a previous global analysis of population exposure to GLOFs[17]. To ensure accurate extraction of population along floodplains, we used a higher-resolution DEM than the 500-m Shuttle Radar Topography Mission (SRTM) DEM that we used for global source-to-sink flow routing described above. Specifically, we downloaded all 5° tiles of the 3″ resolution (~90 m) Multi-Error-Removed Improved-Terrain (MERIT) DEM, which corrects absolute bias, stripe noise, speckle noise and tree height bias in its source datasets (SRTM3 v2.1 and AW3D-30m v1)[101]. For each glacial lake, we routed flow from the lake's central coordinate, clipped the flow path after 50 km downstream distance and buffered the resulting river segment by a 1-km buffer on either side.

To avoid double-counting populations in nested catchments or overlapping river corridors, we dissolved all catchments and river buffers by RGI region, and catchments were clipped from overlapping portions of the river buffers. Population estimates were obtained from four global gridded datasets (for access, see 'Data availability' section). For multitemporal products, we selected the version closest to the target year (2020). These datasets include the Gridded Population of the World, Version 4 (GPWv4) for the year 2020 at 30″ (~1 km) spatial resolution[102]; the Global Human Settlement Layer population grid (GHS-POP, R2023) for 2020 at 3″ (~100 m) resolution[103]; the LandScan dataset for 2020 at 30″ (~1 km) resolution[104]; and the WorldPop dataset

for 2020 at 3″ (~100 m) resolution[105]. We report the median and range (minimum and maximum) of estimated population counts from these four datasets per RGI region, both upstream and downstream of glacial lakes (Fig. 6).

Reporting summary

Further information on research design is available in the Nature Portfolio Reporting Summary linked to this article.

Data availability

Glacial lake polygons were obtained from https://doi.org/10.11888/Cryos.tpdc.300938. The RGI V7.0 (ref. 37) is available via the National Snow and Ice Data Center at https://nsidc.org/data/nsidc-0770/versions/7, and the outlines of the Greenland ice sheet at https://glaciers-cci.enveo.at/crdp2/index.html (ref. 99). Regional summary statistics on glacier thicknesses as of 2017/2018 are available in ref. 39. Glacier elevation change data between 2000 and 2020 can be downloaded from https://doi.org/10.6096/13. We used the Copernicus 30 m DEM (GLO-30) and the ESA land cover maps, both accessed through the Microsoft Planetary Computer (https://planetarycomputer.microsoft.com/dataset/cop-dem-glo-30; https://planetarycomputer.microsoft.com/dataset/io-lulc-annual-v02) using the R Client Library for SpatioTemporal Asset Catalog (rstac)[92]. In addition, we used the HydroSheds DEM (https://www.hydrosheds.org/hydrosheds-core-downloads)[106] and the MERIT DEM[101], available at https://hydro.iis.u-tokyo.ac.jp/~yamadai/MERIT_DEM/. Population data were obtained from four global gridded sources. The LandScan (2020) High Resolution Global Population Dataset was provided by UT-Battelle, LLC, operator of Oak Ridge National Laboratory under contract DE-AC05-00OR22725 with the US Department of Energy, and is available at https://landscan.ornl.gov/. The Gridded Population of the World, Version 4 (GPWv4), Revision 11 (2020), from NASA and CIESIN, is available at https://search.earthdata.nasa.gov/search (ref. 107). WorldPop 2020 (ref. 105) data were produced by the School of Geography and Environmental Science, University of Southampton; Department of Geography and Geosciences, University of Louisville; Département de Géographie, Université de Namur; and CIESIN, Columbia University (2018), funded by the Bill & Melinda Gates Foundation, and are available at https://doi.org/10.5258/SOTON/WP00647. Lastly, the 2020 GHS population grid (R2023)[108] was obtained from the Joint Research Centre of the European Commission at https://human-settlement.emergency.copernicus.eu/download.php?ds=pop. All datasets used in this study were checked for accessibility on 16 June 2025. Supplementary Table 1 provides our compilation of bathymetrically surveyed glacial lakes, including surface areas, bathymetrically derived volumes and references to the underlying data sources. Data to reproduce our analysis and figures are available via Zenodo at https://doi.org/10.5281/zenodo.17896426 (ref. 109).

Code availability

Data were analysed using R version 4.2.2 through the graphical user interface RStudio version 2025.05.1. All codes to reproduce the statistical analysis will be made available via GitHub at https://github.com/geveh/LakeVolumes.

References

1. Huss, M. et al. Toward mountains without permanent snow and ice. *Earth's Future* **5**, 418–435 (2017).
2. The GlaMBIE Team. Community estimate of global glacier mass changes from 2000 to 2023. *Nature* **639**, 382–388 (2025).
3. Marzeion, B., Kaser, G., Maussion, F. & Champollion, N. Limited influence of climate change mitigation on short-term glacier mass loss. *Nat. Clim. Chang.* **8**, 305–308 (2018).
4. Rounce, D. R. et al. Global glacier change in the 21st century: every increase in temperature matters. *Science* **379**, 78–83 (2023).
5. Bosson, J. B. et al. Future emergence of new ecosystems caused by glacial retreat. *Nature* **620**, 562–569 (2023).
6. Carrivick, J. L. & Tweed, F. S. Proglacial lakes: character, behaviour and geological importance. *Quat. Sci. Rev.* **78**, 34–52 (2013).
7. Zhang, T., Wang, W. & An, B. Heterogeneous changes in global glacial lakes under coupled climate warming and glacier thinning. *Commun. Earth Environ.* **5**, 374 (2024).
8. Milner, A. M. et al. Glacier shrinkage driving global changes in downstream systems. *Proc. Natl Acad. Sci. USA* **114**, 9770–9778 (2017).
9. Pritchard, H. D. Asia's shrinking glaciers protect large populations from drought stress. *Nature* **569**, 649–654 (2019).
10. Clague, J. J. & O'Connor, J. E. in *Snow and Ice-related Hazards, Risks, and Disasters* (eds Haeberli, W. & Whitman, C.) 487–519 (Elsevier, 2015).
11. Veh, G. et al. Progressively smaller glacier lake outburst floods despite worldwide growth in lake area. *Nat. Water* **3**, 271–283 (2025).
12. Lützow, N., Veh, G. & Korup, O. A global database of historic glacier lake outburst floods. *Earth Syst. Sci. Data* **15**, 2983–3000 (2023).
13. Zheng, G. et al. Increasing risk of glacial lake outburst floods from future Third Pole deglaciation. *Nat. Clim. Chang.* **11**, 411–417 (2021).
14. Veh, G., Korup, O. & Walz, A. Hazard from Himalayan glacier lake outburst floods. *Proc. Natl Acad. Sci. USA* **117**, 907–912 (2020).
15. Rick, B., McGrath, D., McCoy, S. W. & Armstrong, W. H. Unchanged frequency and decreasing magnitude of outbursts from ice-dammed lakes in Alaska. *Nat. Commun.* **14**, 6138 (2023).
16. Colavitto, B. et al. A glacial lake outburst floods hazard assessment in the Patagonian Andes combining inventory data and case-studies. *Sci. Total Environ.* **916**, 169703 (2024).
17. Taylor, C., Robinson, T. R., Dunning, S., Rachel Carr, J. & Westoby, M. Glacial lake outburst floods threaten millions globally. *Nat. Commun.* **14**, 487 (2023).
18. Zhang, T., Wang, W., An, B. & Wei, L. Enhanced glacial lake activity threatens numerous communities and infrastructure in the Third Pole. *Nat. Commun.* **14**, 8250 (2023).
19. Brunner, M. I. et al. Present and future water scarcity in Switzerland: potential for alleviation through reservoirs and lakes. *Sci. Total Environ.* **666**, 1033–1047 (2019).
20. Purdie, H. Glacier retreat and tourism: insights from New Zealand. *Mt. Res. Dev.* **33**, 463–472 (2013).
21. Viani, C. et al. Socio-environmental value of glacier lakes: assessment in the Aosta Valley (Western Italian Alps). *Reg. Environ. Change* **22**, 7 (2022).
22. Shah, S., Sen, S. & Sahoo, D. State of Indian Northwestern Himalayan lakes under human and climate impacts: a review. *Ecol. Indic.* **160**, 111858 (2024).
23. Motschmann, A., Huggel, C., Muñoz, R. & Thür, A. Towards integrated assessments of water risks in deglaciating mountain areas: water scarcity and GLOF risk in the Peruvian Andes. *Geoenviron. Disasters* **7**, 26 (2020).
24. Farinotti, D., Round, V., Huss, M., Compagno, L. & Zekollari, H. Large hydropower and water-storage potential in future glacier-free basins. *Nature* **575**, 341–344 (2019).
25. Cook, S. J. & Quincey, D. J. Estimating the volume of Alpine glacial lakes. *Earth Surf. Dynam.* **3**, 559–575 (2015).
26. Shugar, D. H. et al. Rapid worldwide growth of glacial lakes since 1990. *Nat. Clim. Chang.* **10**, 939–945 (2020).
27. Muñoz, R., Huggel, C., Frey, H., Cochachin, A. & Haeberli, W. Glacial lake depth and volume estimation based on a large bathymetric dataset from the Cordillera Blanca, Peru. *Earth Surf. Process. Landf.* **45**, 1510–1527 (2020).

28. Emmer, A. & Vilímek, V. New method for assessing the susceptibility of glacial lakes to outburst floods in the Cordillera Blanca, Peru. *Hydrol. Earth Syst. Sci.* **18**, 3461–3479 (2014).

29. Huggel, C., Kääb, A., Haeberli, W., Teysseire, P. & Paul, F. Remote sensing based assessment of hazards from glacier lake outbursts: a case study in the Swiss Alps. *Can. Geotech. J.* **39**, 316–330 (2002).

30. Kapitsa, V. et al. Bathymetries of proglacial lakes: a new data set from the northern Tien Shan, Kazakhstan. *Front. Earth Sci.* **11**, 1192719 (2023).

31. Loriaux, T. & Casassa, G. Evolution of glacial lakes from the Northern Patagonia Icefield and terrestrial water storage in a sea-level rise context. *Glob. Planet. Chang.* **102**, 33–40 (2013).

32. Zhang, G. et al. Underestimated mass loss from lake-terminating glaciers in the greater Himalaya. *Nat. Geosci.* **16**, 333–338 (2023).

33. Cook, S. J. & Swift, D. A. Subglacial basins: Their origin and importance in glacial systems and landscapes. *Earth Sci. Rev.* **115**, 332–372 (2012).

34. Hicks, D. M., MCSaveney, M. J. & Chinn, T. J. H. Sedimentation in Proglacial Ivory Lake, Southern Alps, New Zealand. *Arct. Antarct. Alp. Res.* **22**, 26–42 (1990).

35. Piret, L. et al. Long-lasting impacts of a 20th century glacial lake outburst flood on a Patagonian fjord-river system (Pascua River). *Geomorphology* **399**, 108080 (2022).

36. Fleisher, P. J., Bailey, P. K. & Cadwell, D. H. A decade of sedimentation in ice-contact, proglacial lakes, Bering Glacier. *AK. Sediment. Geol.* **160**, 309–324 (2003).

37. RGI 7.0 Consortium. Randolph Glacier Inventory – A Dataset of Global Glacier Outlines, Version 7.0. *National Snow and Ice Data Center* https://doi.org/10.5067/f6jmovy5navz (2023).

38. Köck, G. et al. Bathymetry and sediment geochemistry of Lake Hazen (Quttinirpaaq National Park, Ellesmere Island, Nunavut). *ARCTIC* **65**, 56–66 (2012).

39. Millan, R., Mouginot, J., Rabatel, A. & Morlighem, M. Ice velocity and thickness of the world's glaciers. *Nat. Geosci.* **14**, 124–129 (2022).

40. Neukom, R., Steiger, N., Gómez-Navarro, J. J., Wang, J. & Werner, J. P. No evidence for globally coherent warm and cold periods over the preindustrial Common Era. *Nature* **571**, 550–554 (2019).

41. Sutherland, J. L., Carrivick, J. L., Shulmeister, J., Quincey, D. J. & James, W. H. M. Ice-contact proglacial lakes associated with the Last Glacial Maximum across the Southern Alps, New Zealand. *Quat. Sci. Rev.* **213**, 67–92 (2019).

42. Kaufman, D. S. & Manley, W. F. in *Developments in Quaternary Sciences* Vol. 2 (eds Ehlers, J. & Gibbard, P. L.) 9–27 (Elsevier, 2004).

43. Caruso, B. S., King, R., Newton, S. & Zammit, C. Simulation of climate change effects on hydropower operations in Mountain Headwater Lakes, New Zealand. *River Res. Appl.* **33**, 147–161 (2017).

44. Li, D. et al. High Mountain Asia hydropower systems threatened by climate-driven landscape instability. *Nat. Geosci.* **15**, 520–530 (2022).

45. Schwanghart, W., Worni, R., Huggel, C., Stoffel, M. & Korup, O. Uncertainty in the Himalayan energy–water nexus: estimating regional exposure to glacial lake outburst floods. *Environ. Res. Lett.* **11**, 074005 (2016).

46. Kenawi, M. S., Alfredsen, K., Stürzer, L. S., Sandercock, B. K. & Bakken, T. H. High-resolution mapping of land use changes in Norwegian hydropower systems. *Renew. Sustain. Energy Rev.* **188**, 113798 (2023).

47. Piret, L. & Bertrand, S. Multidecadal delay between deglaciation and formation of a proglacial lake sediment record. *Quat. Sci. Rev.* **294**, 107752 (2022).

48. Hosmann, S. L. et al. Exploring beneath the retreating ice: swath bathymetry reveals sub- to proglacial processes and longevity of future alpine glacial lakes. *Ann. Glaciol.* **65**, e21 (2025).

49. Emmer, A. Infilled lakes (*Pampas*) of the Cordillera Blanca, Peru: inventory, sediment storage, and paleo outbursts. *Prog. Phys. Geogr. Earth Environ.* **48**, 208–230 (2024).

50. Blöthe, J. H. & Korup, O. Millennial lag times in the Himalayan sediment routing system. *Earth Planet. Sci. Lett.* **382**, 38–46 (2013).

51. Preusser, F., Reitner, J. M. & Schlüchter, C. Distribution, geometry, age and origin of overdeepened valleys and basins in the Alps and their foreland. *Swiss J. Geosci.* **103**, 407–426 (2010).

52. Wilner, J. A. et al. Limits to timescale dependence in erosion rates: quantifying glacial and fluvial erosion across timescales. *Sci. Adv.* **10**, eadr2009 (2024).

53. Finckh, P., Kelts, K. & Lambert, A. Seismic stratigraphy and bedrock forms in perialpine lakes. *Geol. Soc. Am. Bull.* **95**, 1118 (1984).

54. Fabbri, S. C. et al. Subaqueous geomorphology and delta dynamics of Lake Brienz (Switzerland): implications for the sediment budget in the alpine realm. *Swiss J. Geosci.* **114**, 22 (2021).

55. Schiefer, E. & Gilbert, R. Proglacial sediment trapping in recently formed Silt Lake, upper Lillooet Valley, Coast Mountains, British Columbia. *Earth Surf. Process. Landf.* **33**, 1542–1556 (2008).

56. Geilhausen, M., Morche, D., Otto, J.-C. & Schrott, L. Sediment discharge from the proglacial zone of a retreating Alpine glacier. *Z. Geomorphol. Suppl. Issues* **57**, 29–53 (2013).

57. Delaney, I., Bauder, A., Huss, M. & Weidmann, Y. Proglacial erosion rates and processes in a glacierized catchment in the Swiss Alps. *Earth Surf. Process. Landf.* **43**, 765–778 (2018).

58. Morche, D., Katterfeld, C., Fuchs, S. & Schmidt, K.-H. in *Sediment Dynamics and the Hydromorphology of Fluvial Systems* (eds Rowan, J. S., Duck, R. W. & Werritty, A.) 72–81 (IAHS Press, 2006).

59. Steffen, T., Huss, M., Estermann, R., Hodel, E. & Farinotti, D. Volume, evolution, and sedimentation of future glacier lakes in Switzerland over the 21st century. *Earth Surf. Dynam.* **10**, 723–741 (2022).

60. Geertsema, M. et al. The 28 November 2020 landslide, tsunami, and outburst flood—a hazard cascade associated with rapid deglaciation at Elliot Creek, British Columbia, Canada. *Geophys. Res. Lett.* **49**, p.e2021GL096716 (2022).

61. Zhang, T., Wang, W. & An, B. A massive lateral moraine collapse triggered the 2023 South Lhonak Lake outburst flood, Sikkim Himalayas. *Landslides* **5**, 299–311 (2025).

62. Jacquet, J. et al. Hydrologic and geomorphic changes resulting from episodic glacial lake outburst floods: Rio Colonia, Patagonia, Chile. *Geophys. Res. Lett.* **44**, 854–864 (2017).

63. Bogen, J., Xu, M. & Kennie, P. The impact of pro-glacial lakes on downstream sediment delivery in Norway. *Earth Surf. Process. Landf.* **40**, 942–952 (2015).

64. Hinderer, M., Kastowski, M., Kamelger, A., Bartolini, C. & Schlunegger, F. River loads and modern denudation of the Alps—a review. *Earth-Sci. Rev.* **118**, 11–44 (2013).

65. Haeberli, W. & Drenkhan, F. Future lake development in deglaciating mountain ranges. in *Oxford Research Encyclopedia of Natural Hazard Science* (Oxford Univ. Press, 2022); https://doi.org/10.1093/acrefore/9780199389407.013.361

66. Linsbauer, A. et al. Modelling glacier-bed overdeepenings and possible future lakes for the glaciers in the Himalaya—Karakoram region. *Ann. Glaciol.* **57**, 119–130 (2016).

67. Furian, W., Loibl, D. & Schneider, C. Future glacial lakes in High Mountain Asia: an inventory and assessment of hazard potential from surrounding slopes. *J. Glaciol.* **67**, 653–670 (2021).

68. Hugonnet, R. et al. Accelerated global glacier mass loss in the early twenty-first century. *Nature* **592**, 726–731 (2021).

69. Grimes, M., Carrivick, J. L., Smith, M. W. & Comber, A. J. Land cover changes across Greenland dominated by a doubling of vegetation in three decades. *Sci. Rep.* **14**, 3120 (2024).

70. Li, D. et al. Exceptional increases in fluvial sediment fluxes in a warmer and wetter High Mountain Asia. *Science* **374**, 599–603 (2021).

71. Li, D. et al. The competing controls of glaciers, precipitation, and vegetation on high-mountain fluvial sediment yields. *Sci. Adv.* **10**, eads6196 (2024).

72. Messager, M. L., Lehner, B., Grill, G., Nedeva, I. & Schmitt, O. Estimating the volume and age of water stored in global lakes using a geo-statistical approach. *Nat. Commun.* **7**, 13603 (2016).

73. Talukdar, A., Bhattacharya, S., Bandyopadhyay, A. & Dey, A. Microplastic pollution in the Himalayas: Occurrence, distribution, accumulation and environmental impacts. *Sci. Total Environ.* **874**, 162495 (2023).

74. Dong, H. et al. Microplastics in a remote lake basin of the Tibetan Plateau: impacts of atmospheric transport and glacial melting. *Environ. Sci. Technol.* **55**, 12951–12960 (2021).

75. Brander, L. M. et al. Economic values for ecosystem services: a global synthesis and way forward. *Ecosyst. Serv.* **66**, 101606 (2024).

76. Li, X. & Tsigaris, P. The global value of freshwater lakes. *Ecol. Lett.* **27**, e14388 (2024).

77. Immerzeel, W. W. et al. Importance and vulnerability of the world's water towers. *Nature* **577**, 364–369 (2020).

78. Grande Dixence SA. Gornerli multi-purpose reservoir. *Gornerli Multi-Purpose Reservoir* https://www.grande-dixence.ch/en/gornerli-multi-purpose-reservoir-2652/ (2025).

79. Micheletti, N. & Lane, S. N. Water yield and sediment export in small, partially glaciated Alpine watersheds in a warming climate. *Water Resour. Res.* **52**, 4924–4943 (2016).

80. Kumar, R., Pippal, P. S., Raj, A. & Kumar, R. Toxic contaminants in glacial meltwater and their impact on the environment and human health. *Water Conserv. Sci. Eng.* https://doi.org/10.1007/s41101-025-00379-8 (2025).

81. Moulton, H., Carey, M., Huggel, C. & Motschmann, A. Narratives of ice loss: new approaches to shrinking glaciers and climate change adaptation. *Geoforum* **125**, 47–56 (2021).

82. Zhang, G. et al. Characteristics and changes of glacial lakes and outburst floods. *Nat. Rev. Earth Environ.* **5**, 447–462 (2024).

83. Bürkner, P.-C. brms: An R package for Bayesian multilevel models using Stan. *J. Stat. Soft.* **80**, 1–28 (2017).

84. *Stan Modeling Language Users Guide and Reference Manual* (Stan Development Team, 2022).

85. Song, C., Fan, C., Ma, J., Zhan, P. & Deng, X. A spatially constrained remote sensing-based inventory of glacial lakes worldwide. *Sci. Data* **12**, 464 (2025).

86. Emmer, A., Merkl, S. & Mergili, M. Spatiotemporal patterns of high-mountain lakes and related hazards in western Austria. *Geomorphology* **246**, 602–616 (2015).

87. Emmer, A. et al. 70 years of lake evolution and glacial lake outburst floods in the Cordillera Blanca (Peru) and implications for the future. *Geomorphology* **365**, 107178 (2020).

88. Maharjan, S. B. et al. *The Status of Glacial Lakes in the Hindu Kush Himalaya-ICIMOD Research Report 2018/1* (ICIMOD, 2018).

89. Wilson, R. et al. Glacial lakes of the Central and Patagonian Andes. *Glob. Planet. Chang.* **162**, 275–291 (2018).

90. Farinotti, D. et al. A consensus estimate for the ice thickness distribution of all glaciers on Earth. *Nat. Geosci.* **12**, 168–173 (2019).

91. Microsoft Open Source, McFarland, M., Emanuele, R. Morris, D. & Augspurger, T. microsoft/PlanetaryComputer. *Zenodo* https://doi.org/10.5281/zenodo.7261897 (2022).

92. Simoes, R. et al. Rstac: an R package to access spatiotemporal asset catalog satellite imagery. In *2021 IEEE International Geoscience and Remote Sensing Symposium IGARSS* 7674–7677 (IEEE, 2021); https://doi.org/10.1109/igarss47720.2021.9553518

93. Schwanghart, W. & Scherler, D. Short Communication: TopoToolbox 2—MATLAB-based software for topographic analysis and modeling in Earth surface sciences. *Earth Surf. Dynam.* **2**, 1–7 (2014).

94. Lehner, B., Verdin, K. & Jarvis, A. New global hydrography derived from spaceborne elevation data. *EoS Trans.* **89**, 93–94 (2008).

95. Daly, R. A., Manger, G. E. & Clark, S. P. in *Geological Society of America Memoir* Vol. 97 (ed Clark, S. P.) 19–26 (Geological Society of America, 1966).

96. Verstraeten, G. & Poesen, J. Estimating trap efficiency of small reservoirs and ponds: methods and implications for the assessment of sediment yield. *Prog. Phys. Geogr.* **24**, 219–251 (2000).

97. Liermann, S., Beylich, A. A. & Van Welden, A. Contemporary suspended sediment transfer and accumulation processes in the small proglacial Sætrevatnet sub-catchment, Bødalen, western Norway. *Geomorphology* **167–168**, 91–101 (2012).

98. Avnimelech, Y., Ritvo, G., Meijer, L. E. & Kochba, M. Water content, organic carbon and dry bulk density in flooded sediments. *Aquac. Eng.* **25**, 25–33 (2001).

99. Rastner, P. et al. The first complete inventory of the local glaciers and ice caps on Greenland. *Cryosphere* https://doi.org/10.5194/tc-6-1483-2012 (2012).

100. Xu, P. et al. Comparative validation of recent 10 m-resolution global land cover maps. *Remote Sens. Environ.* **311**, 114316 (2024).

101. Yamazaki, D. et al. A high-accuracy map of global terrain elevations. *Geophys. Res. Lett.* **44**, 5844–5853 (2017).

102. Doxsey-Whitfield, E. et al. Taking advantage of the improved availability of census data: a first look at the gridded population of the world, version 4. *Pap. Appl. Geogr.* **1**, 226–234 (2015).

103. Pesaresi, M. et al. Advances on the Global Human Settlement Layer by joint assessment of Earth Observation and population survey data. *Int. J. Digit. Earth* **17**, 2390454 (2024).

104. Dobson, J. E., Bright, E. A., Coleman, P. R., Durfee, R. C. & Worley, B. A. LandScan: a global population database for estimating populations at risk. *Photogramm. Eng. Remote Sens.* **66**, 849–857 (2000).

105. Tatem, A. J. WorldPop, open data for spatial demography. *Sci. Data* **4**, 170004 (2017).

106. Lehner, B., Verdin, K. & Jarvis, A. New global hydrography derived from spaceborne elevation data. *Eos* **89**, 93–94 (2008).

107. Center For International Earth Science Information Network-CIESIN-Columbia University. *Gridded Population of the World, Version 4 (GPWv4): Population Density, Revision 11 (Version 4.11)* (NASA Socioeconomic Data and Applications Center, 2017); https://doi.org/10.7927/H49C6VHW

108. Carioli, A., Schiavina, M., MacManus, K. J., & Freire, S. *GHS-POP R2023A – GHS population grid multitemporal (1975–2030)* (European Commission, Joint Research Centre, 2023); https://doi.org/10.2905/2FF68A52-5B5B-4A22-8F40-C41DA8332CFE

109. Veh, G. Supplementary data for 'Evolving resource potential of glacial lakes with ongoing deglaciation'. *Zenodo* https://doi.org/10.5281/zenodo.17896427 (2025).

Acknowledgements

Author contributions

G.V. designed and led the study, analysed the data, produced all figures and wrote the manuscript. W.S. derived flow paths downstream

Competing interests

The authors declare no competing interests.

Additional information

Extended data is available for this paper at https://doi.org/10.1038/s44221-025-00578-6.

Supplementary information The online version contains supplementary material available at https://doi.org/10.1038/s44221-025-00578-6.

Correspondence and requests for materials should be addressed to Georg Veh.

Peer review information *Nature Water* thanks Simon Cook and the other, anonymous, reviewer(s) for their contribution to the peer review of this work.

Reprints and permissions information is available at www.nature.com/reprints.

Publisher's note Springer Nature remains neutral with regard to jurisdictional claims in published maps and institutional affiliations.

Extended Data Fig. 1 | Posterior predictive distributions for the five dam types. a, Predictions for each dam type from the hierarchical Bayesian regression model. Label (*n*) is the sample size per group. **b**, Posterior distribution of the regression intercept (left panel) and slope (right panel) for each dam type for $\log_{10}$-transformed input data. A one-unit change in either parameter corresponds to a tenfold (one-order-of-magnitude) change. White circles with red outlines are the medians per dam type, and horizontal black embrace the 68 % HDIs. The solid vertical grey line is the posterior median on population level, and dashed lines denotes its 68 % HDI. Both intercept and slope for moraine-dammed lakes is credibly larger than for the other dam types and the pooled estimate.
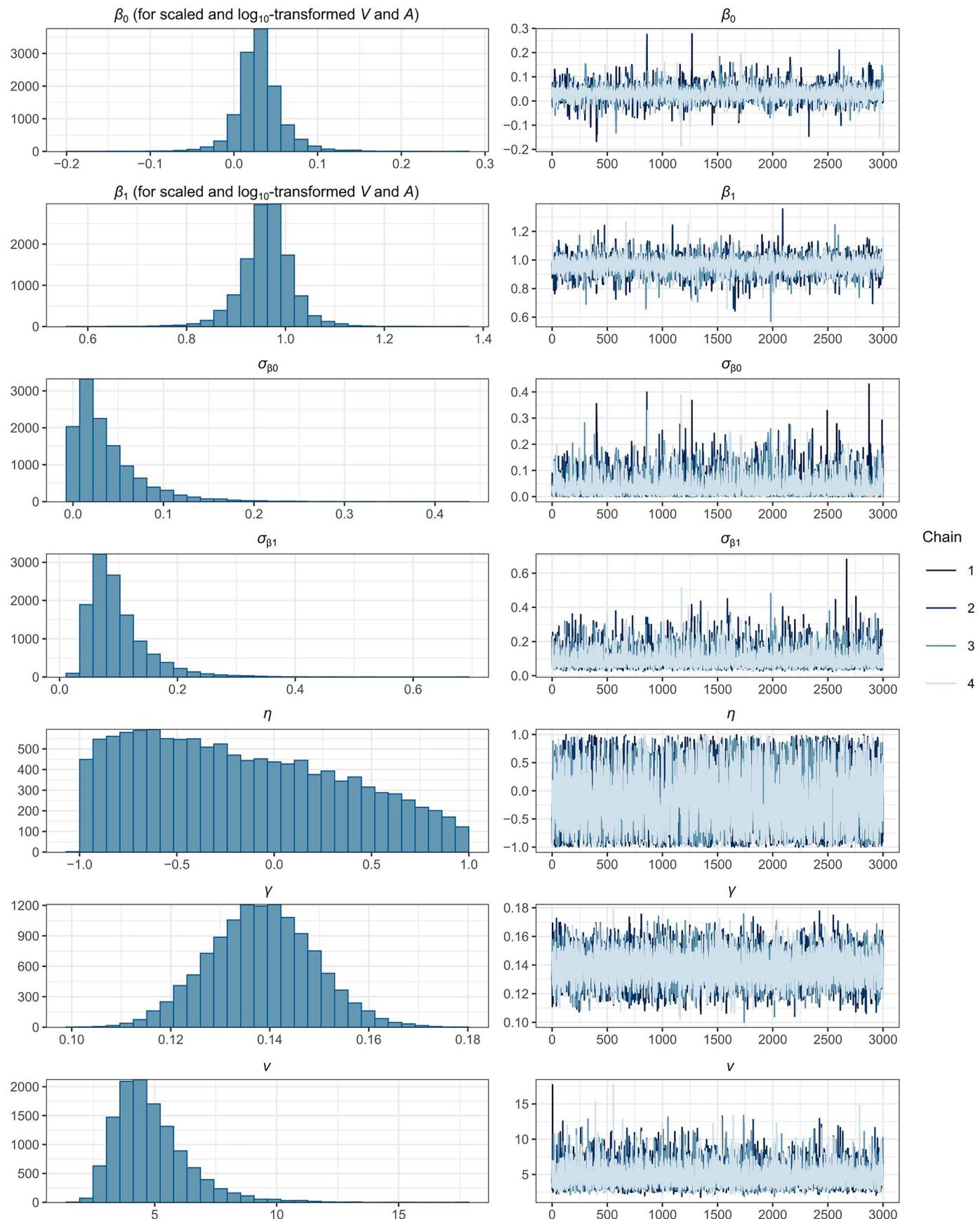
**Extended Data Fig. 2 | Posterior distributions and sample diagnostics of the parameters in the hierarchical *V-A* regression model.** Each row shows the histogram of the posterior distribution of a given parameter (left) that is aggregated from 4 parallel Markov Monte Carlo chains (right). Symbols are explained in the Methods.
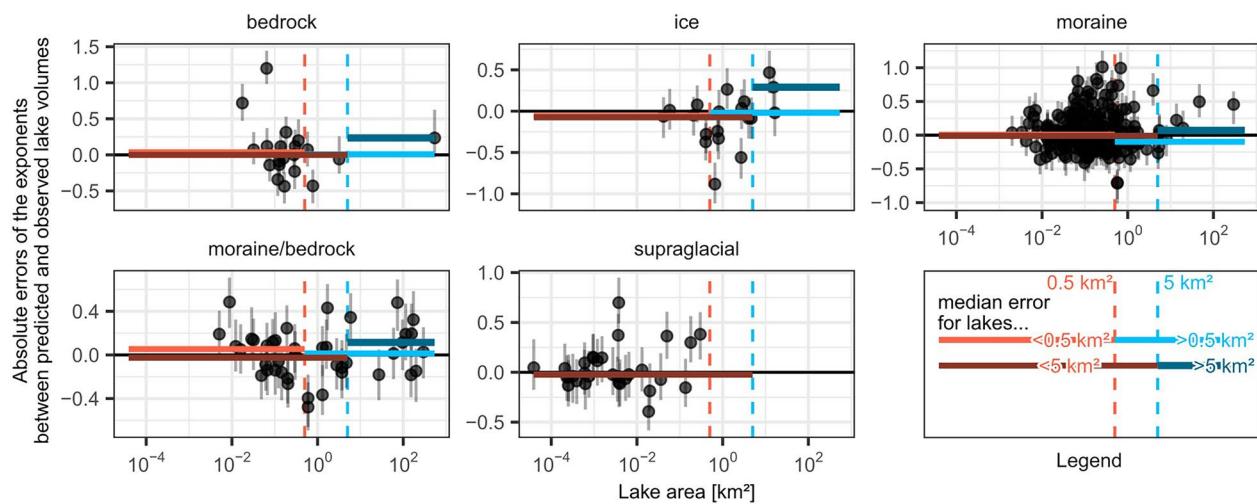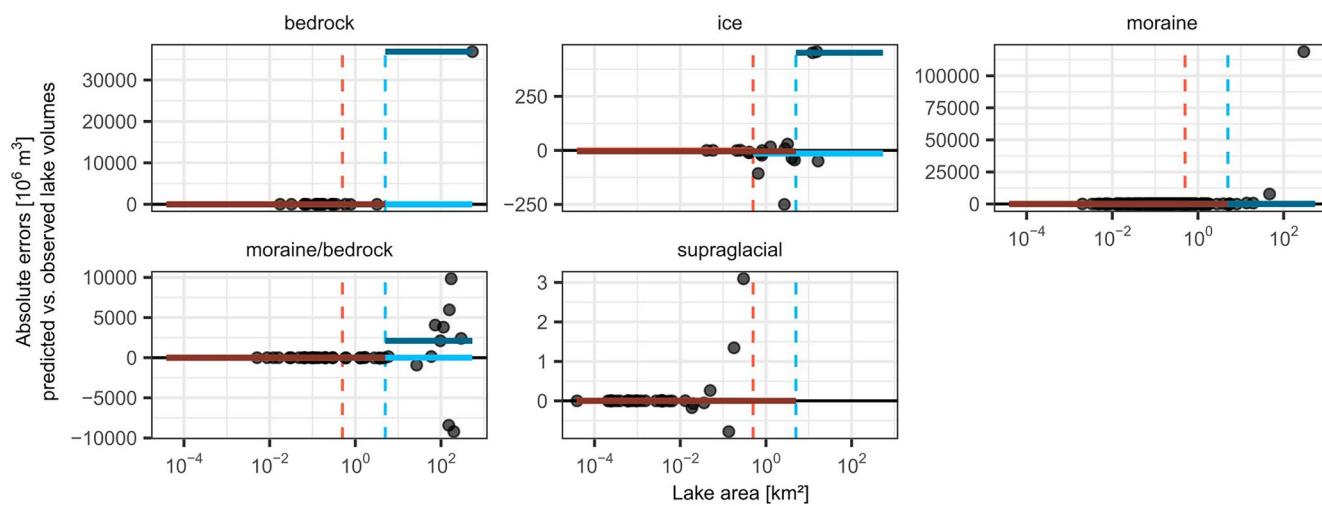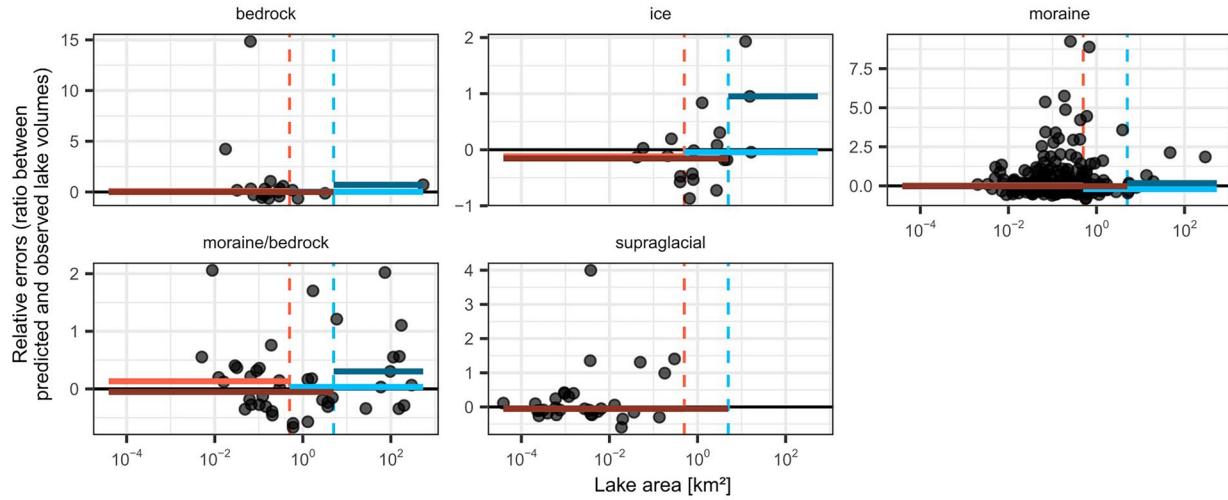
Extended Data Fig. 3 | Error assessment of the hierarchical *V-A* model. We evaluate the median difference between observed and predicted lake volumes on either side of the suspected breakpoints at *A* = 0.5 km² (light red and light blue lines) or *A* = 5 km² (dark red and dark blue lines). Legend in the top right applies to all panels. **a**, Absolute errors for log₁₀-transformed data (that is, the direct output of the *V-A* model). These errors represent differences in exponents between observation and prediction, effectively showing errors in terms of orders of magnitude. **b**, Absolute errors after back-transforming the median predicted volume to the original scale, measured in 10⁶ m³. **c**, Relative errors, expressed as the ratio between predicted and observed lake volume. Positive values indicate an *n*-fold overestimation, while negative values indicate an *n*-fold underestimation.
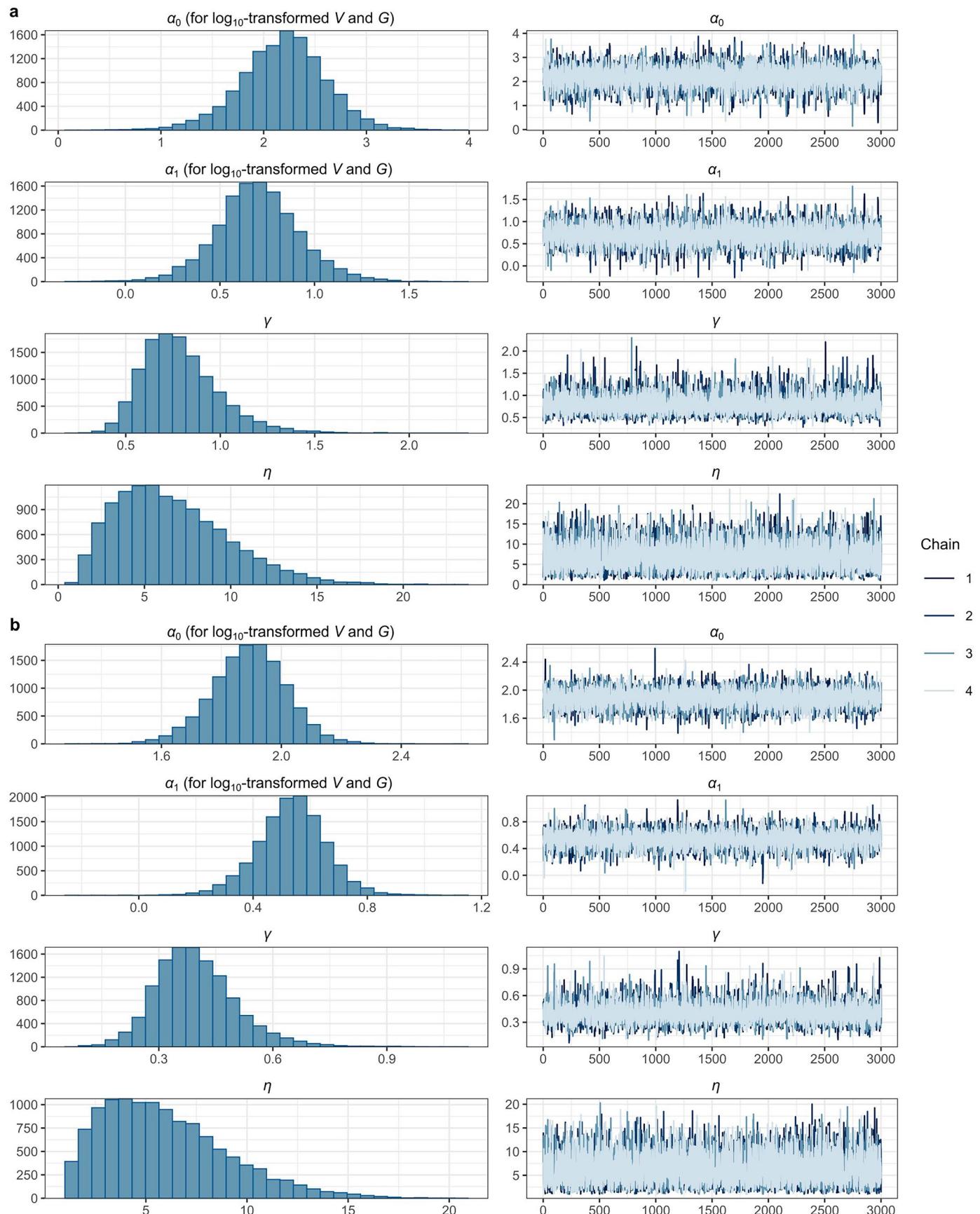
Extended Data Fig. 4 | Posterior distributions and sample diagnostics of the parameters in the regression models that predict glacier volume (change) from lake volume (change). a, Regional glacier volume predicted from regional lake volume. **b**, Regional glacier volume loss predicted from regional lake volume change. Each row shows the histogram of the posterior distribution of a given parameter (left) that is aggregated from 4 parallel Markov Monte Carlo chains (right) with 3,000 draws after warm-up each. Greek symbols are explained in the Methods.
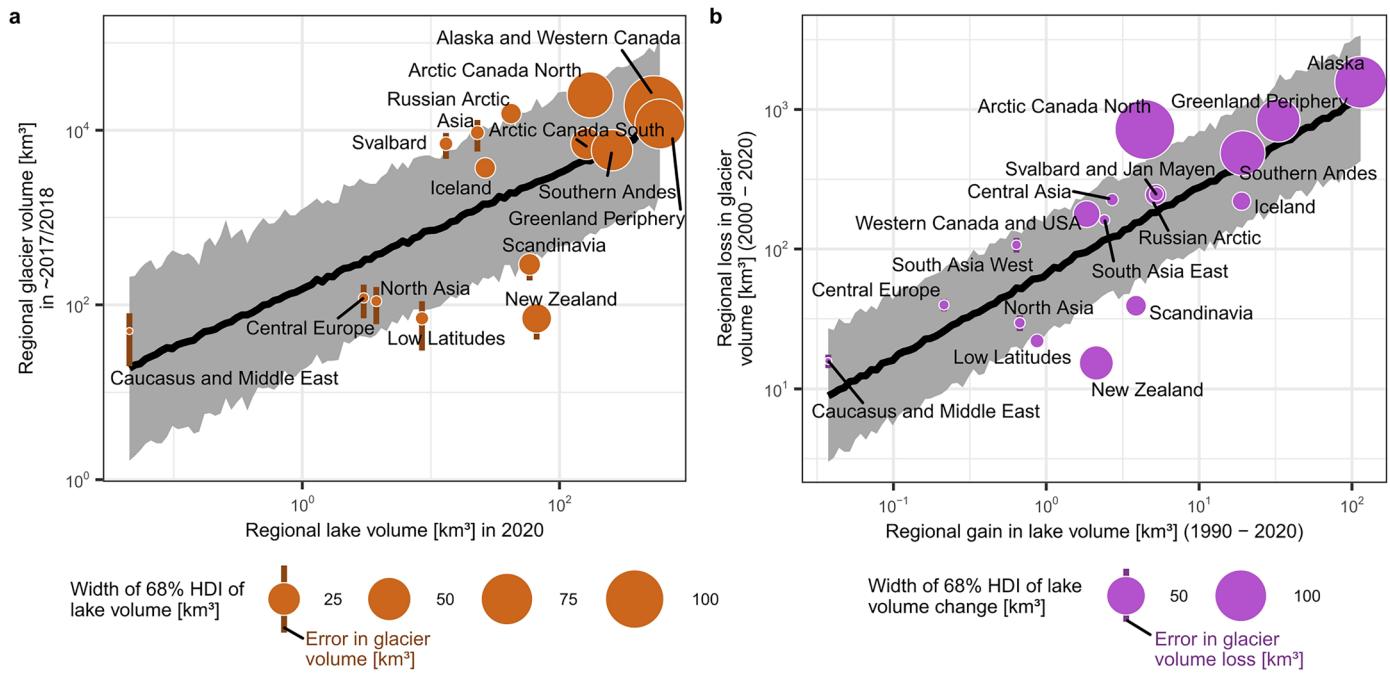
Extended Data Fig. 5 | Trends of lake volume (change) with glacier volume (change). a, Regional glacier volume[41] averaged for the period 2017-2018 predicted from regional lake volumes in 2020. **b**, Regional glacier volume loss in 2000-2020 (ref. 69) predicted from regional increases in lake volume. Vertical bars show the 1σ error in regional glacier volumes[41] (**a**) and glacier volumes loss[69]

(**b**). Bubble size scales with the uncertainties in lake volume (**a**) and lake volume increase (**b**). The linear regression model in the background is summarised by the median (black line) and the 68% HDI (grey shade) of the posterior predictive distribution.
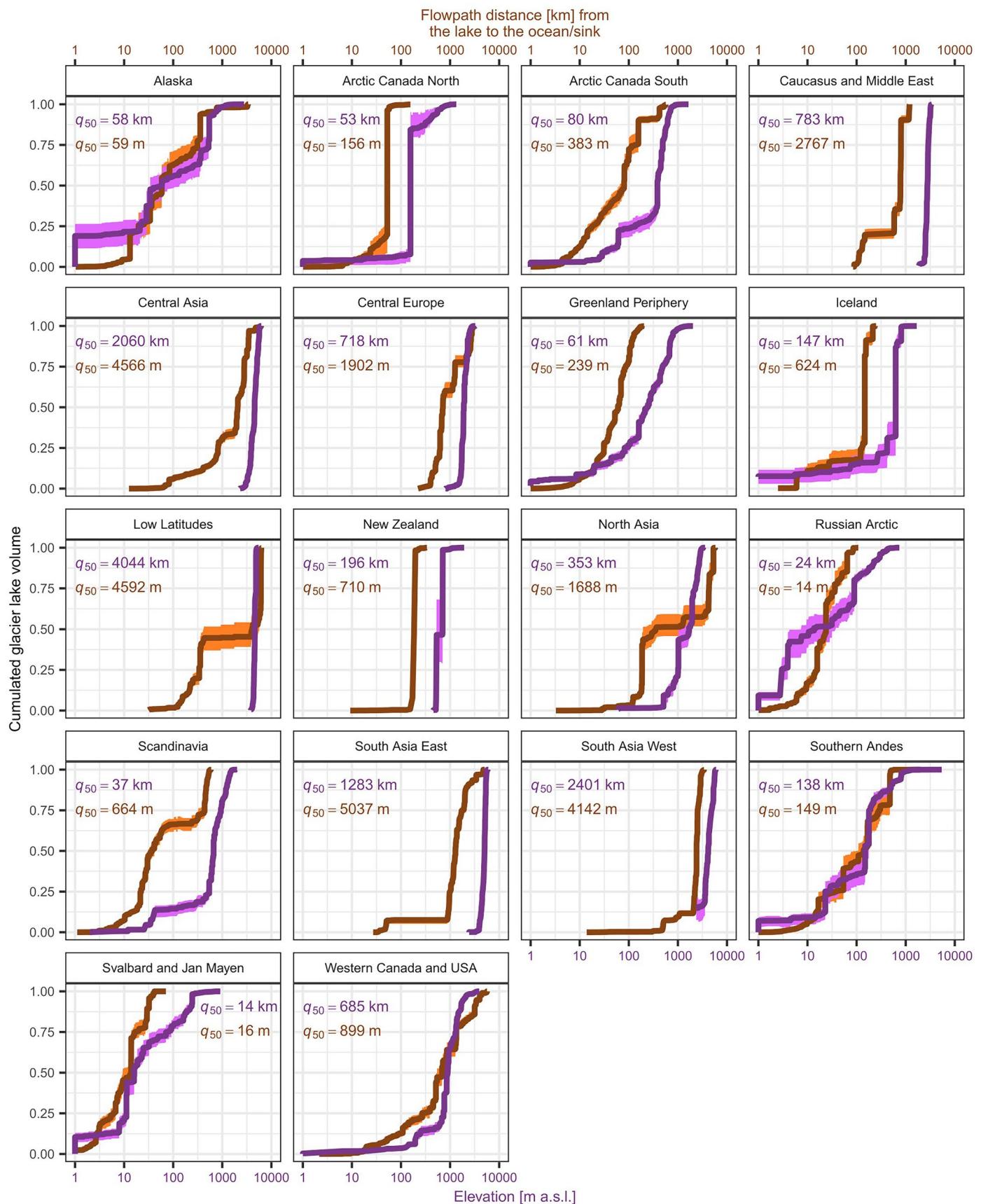
Extended Data Fig. 6 | Regional cumulated glacial lake volumes with elevation and flowpath distance to the coast. Cumulated glacial lake volumes are sorted by elevation (purple) and flowpath distance (orange) to the ocean or sink, if lakes drain into endorheic basins. Lines are the median cumulated volume and shades are the 68% HDI. Color-coded labels mark the elevation or downstream distance at which 50% (q_{50}) of the total volume is reached.
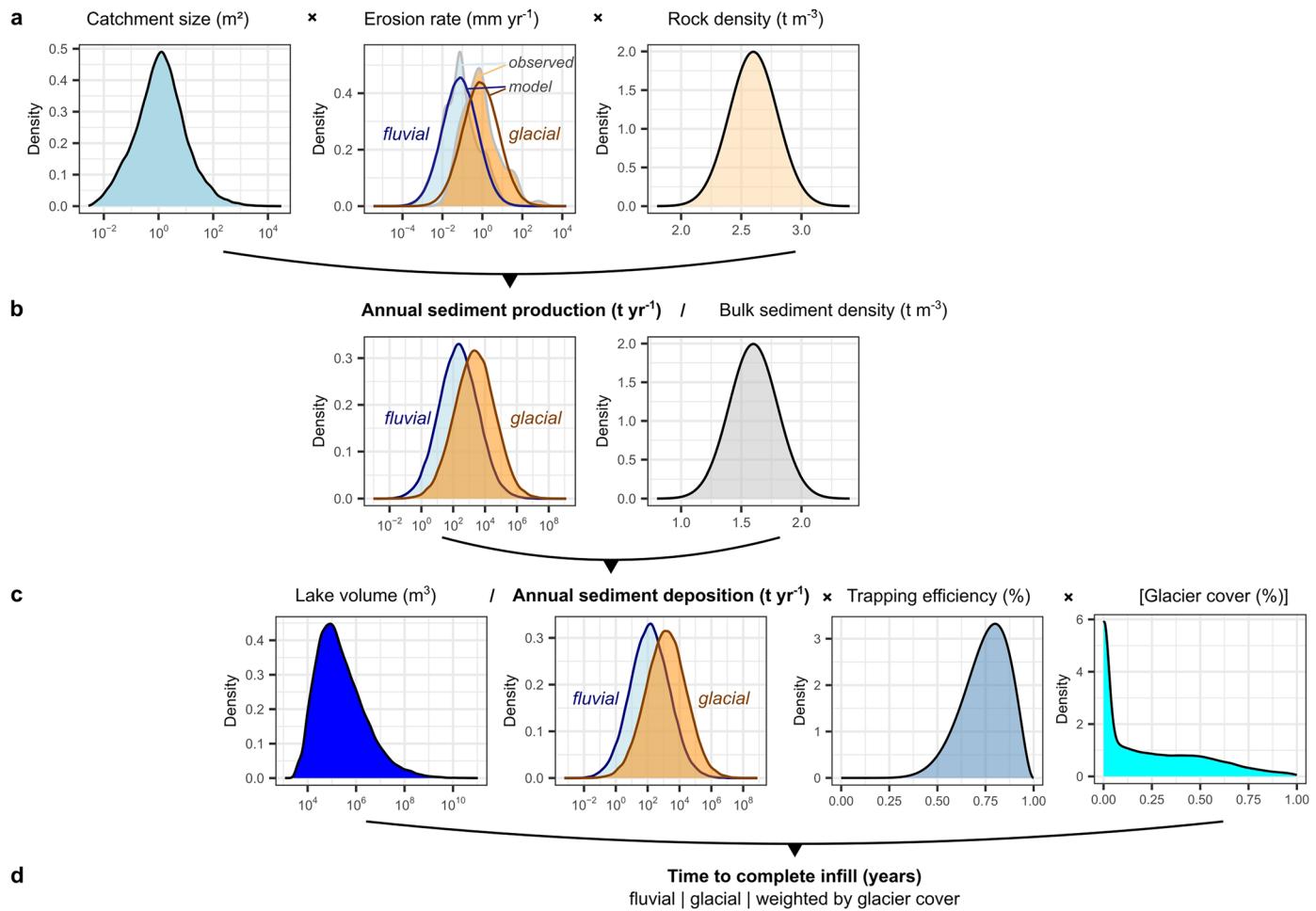
Extended Data Fig. 7 | Schematic diagram of glacial lake lifetime estimation for 59,090 proglacial lakes mapped in 2020. For each lake, only the catchment size (**a**) and glacier cover (**c**) are fixed, while all other parameters are sampled 5,000 times from their respective distributions. **a**, Annual sediment production is calculated as the product of catchment area, reported erosion rates[59], and rock density. **b**, Sediment production is converted to annual sediment deposition by dividing by the bulk sediment density. **c**, The deposition is corrected for sediment trapping efficiency as portion of sediment bypasses the lake. **d**, The lake lifetime is then estimated by dividing the lake volume by the product of annual sediment deposition and trapping efficiency. Besides end-member scenarios for fully fluvial or glacial erosion rates, each sample is also weighted by the glacier cover in the catchment to account for transitions in erosion regimes.
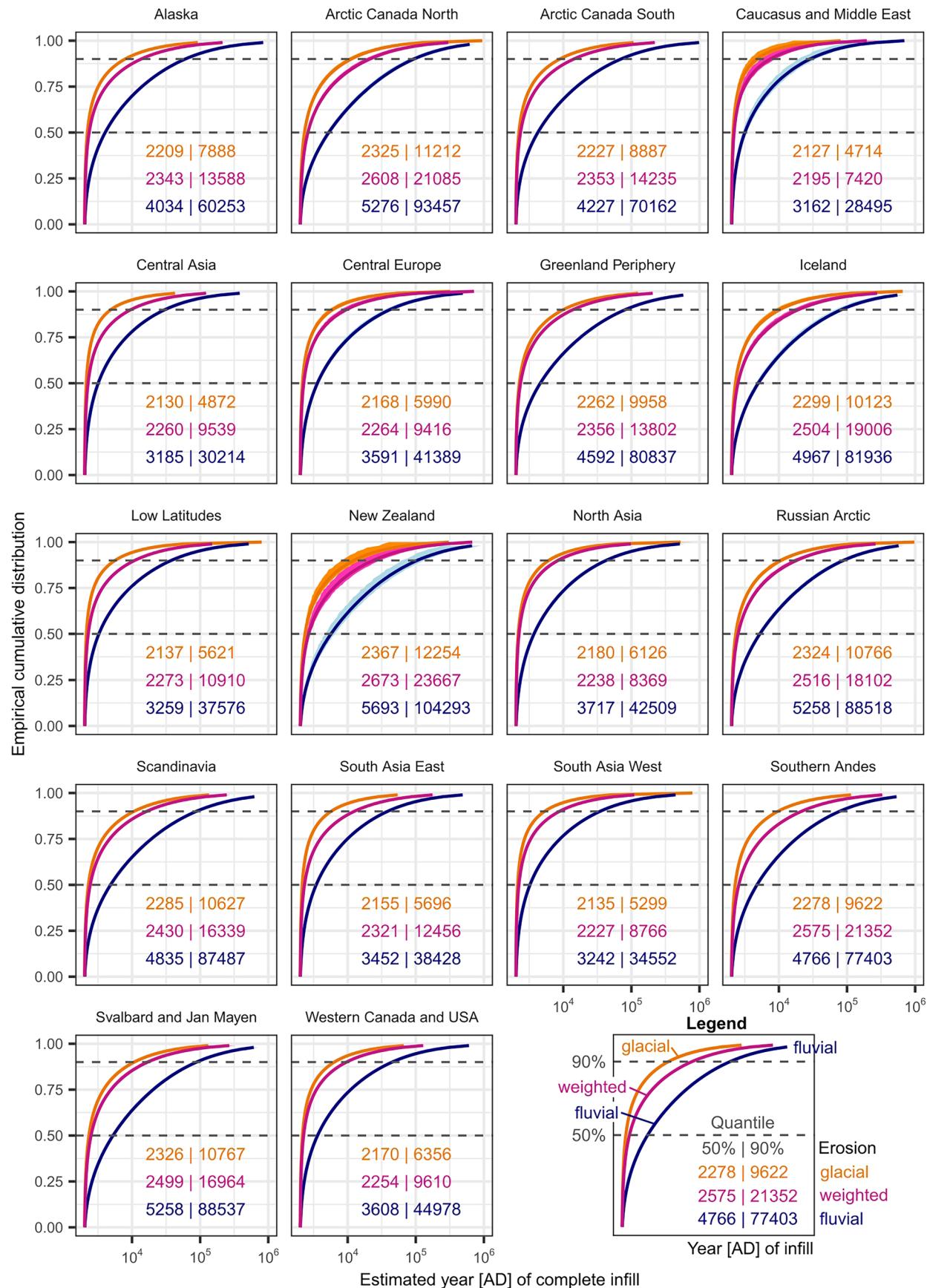
Extended Data Fig. 8 | Estimated year of lake infill under glacial, fluvial, and intermediate erosion scenarios. For each region, we show the cumulative distribution of glacial lake lifespans based on 5,000 simulations. Color-coded numbers indicate the median year by which 10% (left), 25% (middle) and 50% (right) of all lakes in a region are projected to be completely filled under glacial (orange) and fluvial (blue) erosion rates. Purple labels and lines represent a weighted scenario, in which erosion rates are scaled by glacier cover in each lake's catchment.
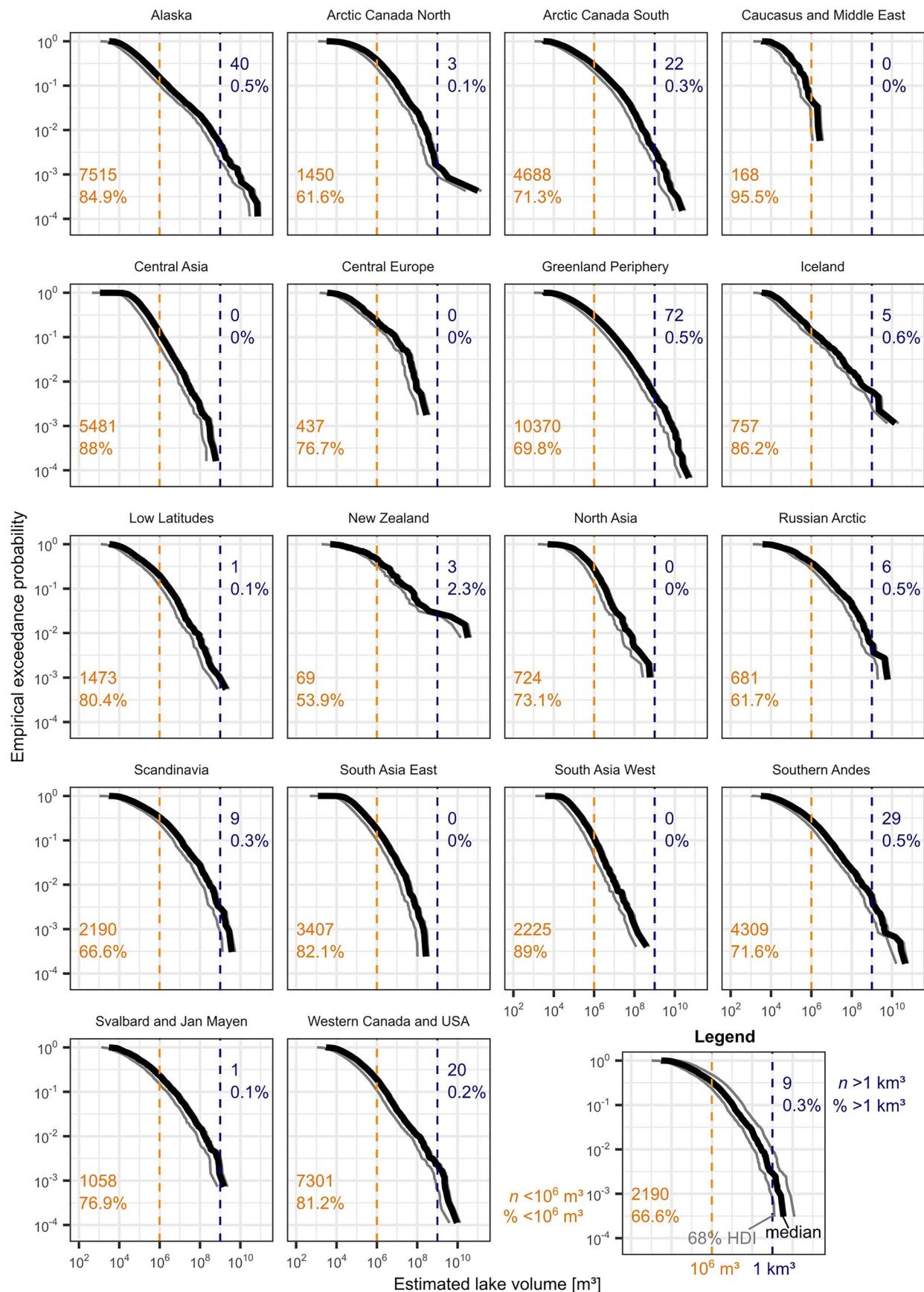
Extended Data Fig. 9 | Volume and frequency of glacial lakes as of 2020 across 18 study regions. Black lines show posterior lake volumes ranked by empirical exceedance probability; grey lines indicate the 68% highest density interval (HDI) of the posterior distribution. Dashed vertical orange lines and labels mark the regional number (top) and percentage (bottom) of lakes with volumes <1 million m³; blue dashed vertical lines and labels show same statistics for lakes >1 km³.
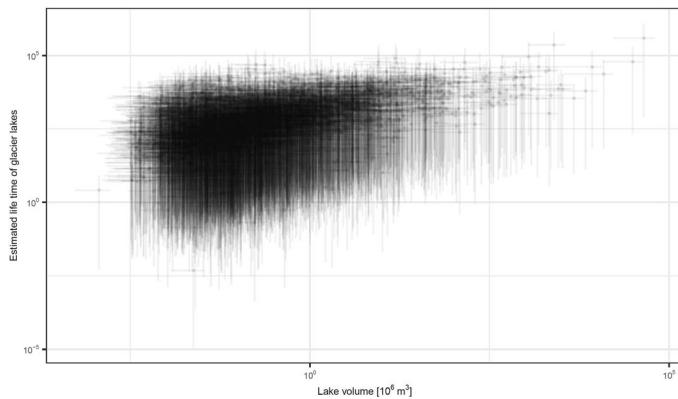
Extended Data Fig. 10 | Lake volume versus their estimated lifetime until complete infill of 59,090 proglacial lakes as of 2020. We exclude supraglacial lakes and summarise both distributions using the median (dots) and the 68% HDI.

nature portfolio

Corresponding author(s): Georg Veh

Last updated by author(s): Dec 10, 2025

Reporting Summary

Nature Portfolio wishes to improve the reproducibility of the work that we publish. This form provides structure for consistency and transparency in reporting. For further information on Nature Portfolio policies, see our Editorial Policies and the Editorial Policy Checklist.

Statistics

For all statistical analyses, confirm that the following items are present in the figure legend, table legend, main text, or Methods section.

n/a	Confirmed	
☐	☒	The exact sample size (*n*) for each experimental group/condition, given as a discrete number and unit of measurement
☐	☒	A statement on whether measurements were taken from distinct samples or whether the same sample was measured repeatedly
☒	☐	The statistical test(s) used AND whether they are one- or two-sided *Only common tests should be described solely by name; describe more complex techniques in the Methods section.*
☐	☒	A description of all covariates tested
☐	☒	A description of any assumptions or corrections, such as tests of normality and adjustment for multiple comparisons
☐	☒	A full description of the statistical parameters including central tendency (e.g. means) or other basic estimates (e.g. regression coefficient) AND variation (e.g. standard deviation) or associated estimates of uncertainty (e.g. confidence intervals)
☒	☐	For null hypothesis testing, the test statistic (e.g. *F*, *t*, *r*) with confidence intervals, effect sizes, degrees of freedom and *P* value noted *Give P values as exact values whenever suitable.*
☐	☒	For Bayesian analysis, information on the choice of priors and Markov chain Monte Carlo settings
☐	☒	For hierarchical and complex designs, identification of the appropriate level for tests and full reporting of outcomes
☒	☐	Estimates of effect sizes (e.g. Cohen's *d*, Pearson's *r*), indicating how they were calculated

Our web collection on statistics for biologists contains articles on many of the points above.

Software and code

Policy information about availability of computer code

Data collection	River flow paths were derived using the software package TopoToolbox3 in Matlab R2023b. Catchments of lakes were derived using SAGA GIS Version 9.6.1
Data analysis	Data were analysed using R version 4.2.2 through the graphical user interface RStudio 2025.05.1. Our code is deposited on GitHub: https://github.com/geveh/LakeVolumes

For manuscripts utilizing custom algorithms or software that are central to the research but not yet described in published literature, software must be made available to editors and reviewers. We strongly encourage code deposition in a community repository (e.g. GitHub). See the Nature Portfolio guidelines for submitting code & software for further information.

Data

Policy information about availability of data

All manuscripts must include a data availability statement. This statement should provide the following information, where applicable:
- Accession codes, unique identifiers, or web links for publicly available datasets
- A description of any restrictions on data availability
- For clinical datasets or third party data, please ensure that the statement adheres to our policy

Glacial lake polygons were obtained from https://doi.org/10.11888/Cryos.tpdc.300938. The Randolph Glacier Inventory V7.0 (ref. 37) is available from the National Snow and Ice Data Center at https://nsidc.org/data/nsidc-0770/versions/7, and the outlines of the Greenland ice sheet at https://glaciers-cci.enveo.at/crdp2/

Research involving human participants, their data, or biological material

Policy information about studies with **human participants or human data**. See also policy information about **sex, gender (identity/presentation), and sexual orientation** and **race, ethnicity and racism**.

Reporting on sex and gender	Not applicable
Reporting on race, ethnicity, or other socially relevant groupings	Not applicable
Population characteristics	Not applicable
Recruitment	Not applicable
Ethics oversight	Not applicable

Note that full information on the approval of the study protocol must also be provided in the manuscript.

Field-specific reporting

Please select the one below that is the best fit for your research. If you are not sure, read the appropriate sections before making your selection.

☐ Life sciences   ☐ Behavioural & social sciences   ☒ Ecological, evolutionary & environmental sciences

For a reference copy of the document with all sections, see nature.com/documents/nr-reporting-summary-flat.pdf

Ecological, evolutionary & environmental sciences study design

All studies must disclose on these points even when the disclosure is negative.

Study description	We quantified the volume and theoretical lifetime of each glacier lake worldwide. We used a global dataset of glacier lake outlines that were mapped from satellite imagery taken in 1990 and 2020 by Zhang et al. (2024). Lake volumes were estimated using a Bayesian hierarchical area–volume regression model, drawing on a compilation of 321 bathymetrically surveyed lakes. To constrain potential sediment infill, we combined lake catchments (derived from digital elevation models) with reported data of catchment-wide erosion rates (Wilner et al., 2024). Lake lifetimes were then approximated by modelling the timespan when expected sediment delivery equals the the current (2020) lake volume. Social implications of changing lake volumes were inferred from the estimated number of people living in the upstream contributing catchments, as well as in the first 50 km downstream of lakes, using four gridded datasets of population counts (see Data availability statement).
Research sample	Digitized glacier lake polygons in 1990 (n = 46,422) and 2024 (n = 70,862) were obtained from Zhang et al. (2024), Nature Communications https://doi.org/10.11888/Cryos.tpdc.300938. Lakes were assigned to a given glaciated mountain region according to the Randolph Glacier Inventory V7.0 , available from the National Snow and Ice Data Center at https://nsidc.org/data/nsidc-0770/versions/7. Bathymetrically surveyed glacier lakes were collected in an Excel Spreadsheet, including their surface areas, bathymetrically derived volumes, and references to the underlying data sources, see Supplementary Dataset. We compare regional estimates of glacier lake volumes with regional summary statistics on glacier thicknesses as of 2017/2018 as reported in Millan et al. (2022), Nature Geoscience. We also compare changes in glacier lake volumes between 1990 and 2020 with glacier elevation change data between 2000 and 2020, as reported in Hugonnet et al. (2021), available at https://doi.org/10.6096/13. Lake and catchment characteristics (such as elevation of the lake, area of the catchment, or landcover) for all lakes reported in Zhang et al. (2024) were derived from the Copernicus 30m digital elevetion model (DEM) (GLO-30) and the ESA land cover maps, both accessed through the Microsoft Planetary Computer (https://planetarycomputer.microsoft.com/dataset/cop-dem-glo-30; https://

planetarycomputer.microsoft.com/dataset/io-lulc-annual-v02). Downstream flowpaths of glacier lakes were derived from the HydroSheds DEM (https://www.hydrosheds.org/hydrosheds-core-downloads) and the MERIT DEM, available from https://hydro.iis.u-tokyo.ac.jp/~yamadai/MERIT_DEM/.

Population data up- and downstream of glacier lakes were obtained from four global gridded (i.e. rasterized) sources. The LandScan (2020)™ High Resolution Global Population Dataset was provided by UT-Battelle, LLC, operator of Oak Ridge National Laboratory under contract DE-AC05-00OR22725 with the U.S. Department of Energy, and is available at https://landscan.ornl.gov/. The Gridded Population of the World, Version 4 (GPWv4), Revision 11 (2020), from NASA and CIESIN, is available at https://search.earthdata.nasa.gov/search. WorldPop 2020 data were produced by the School of Geography and Environmental Science, University of Southampton; Department of Geography and Geosciences, University of Louisville; Département de Géographie, Université de Namur; and CIESIN, Columbia University (2018), funded by the Bill & Melinda Gates Foundation, and are available at https://dx.doi.org/10.5258/SOTON/WP00647. Lastly, the 2020 GHS population grid (R2023) was obtained from the Joint Research Centre of the European Commission at https://human-settlement.emergency.copernicus.eu/download.php?ds=pop.

Sampling strategy

No sample-size calculation was performed. We used all available data in our Bayesian hierarchial regression models.

Data collection

The area and volume of bathymetrically surveyed lakes were compiled by the first author (Georg Veh) from previous studies, and we report the underlying sources in the Supplementary Dataset.

Timing and spatial scale

The glacial lakes in our global sample were bathymetrically surveyed between 1961 and 2024 (see Supplementary Table 1). These lakes are located in various glaciated mountain regions, including - among others - the Andes, the European and Southern Alps, High Mountain Asia, the Coast Mountains ain NW North America, and Scandinavia. The regression model of lake area vs. volume was used to predict the volume of all lakes in 1990 and 2020 worldwide mapped in Zhang et al. (2024). Regional lake volumes were aggregated according to the regional outlines given in the Randolph Glacier Inventory V7.0.

Data exclusions

We did not exclude data intentionally from our analysis. Our regression models used the volume and area of all glacial lakes that we were able to access in published articles. The prediction of theoretical lifetimes of glacier lakes does not include supraglacial lakes as we deem them to be short-lived features.

Reproducibility

Our Bayesian use Markov chain Monte Carlo (MCMC) sampling to approximate the posterior distributions. This approach at randomization, but the posterior is more robustly approximated with increasing number of steps. We used 4000 steps per chain and did not notice any differences when repeatedly running the same model.

Randomization

Bathymetrically surveyed glacial lakes in Supplementary Table 1 were assigned a dam type (supraglacial, moraine, bedrock, ice, or moraine/bedrock) according to the underlying study, or if not mentioned explicitly, by visual analysis of satellite images. The digital outlines of lakes in Zhang et al. (2024) explicitly distiniguish between ice- and non-ice dammed lakes. For the non-ice dammed lakes, we assigned those located entirely within glacier boundaries of the RGI 7.0 as supraglacial lakes and randomly assigned the remaining lakes to one of those classes.

Blinding

Not applicable

Did the study involve field work? ☐ Yes ☒ No

Reporting for specific materials, systems and methods

We require information from authors about some types of materials, experimental systems and methods used in many studies. Here, indicate whether each material, system or method listed is relevant to your study. If you are not sure if a list item applies to your research, read the appropriate section before selecting a response.

Materials & experimental systems

n/a	Involved in the study
☒	Antibodies
☒	Eukaryotic cell lines
☒	Palaeontology and archaeology
☒	Animals and other organisms
☒	Clinical data
☒	Dual use research of concern
☒	Plants

Methods

n/a	Involved in the study
☒	ChIP-seq
☒	Flow cytometry
☒	MRI-based neuroimaging

Plants

Seed stocks

Not applicable

Novel plant genotypes

Not applicable

Authentication

Not applicable